The Nonlinear Universe – Solitons and Chaos

Sai Venkatesh Balasubramanian
Sree Sai Vidhya Mandhir, Mallasandra, Bengaluru-560109, Karnataka, India
saivenkateshbalasubramanian@gmail.com

Abstract:

In this article, two of the pinnacles of nonlinear science – solitons and chaos, are discussed giving importance to the philosophy behind these concepts, and highlighting the ubiquity of the duo in real life phenomena. It is seen that solitons and chaos are prevalent in nature much more than one would expect, and are much wider in scope than the restrictive mathematical equations usually seen in literature. While solitons are a representation of the fundamental life cycle of birth, growth, zenith, decay and death, chaos is seen as a representation of the amount of information an observer possesses, and the interconnectedness between everything and everything else. Various applications of the soliton in communications and computing are discussed. The smoothness and compactness of the soliton give rise to its involvement in various phenomena in nature, along with the genesis of the 'solitary wavelet'. With the characteristic signatures of determinism and sensitive dependence on initial conditions, chaos theory forms the hallmark of nonlinear science. The present work stresses on and elaborates various techniques on achieving an easy-to-tune signal based chaos, with the help of standard circle maps, mathematical functions and digital circuits. Following this various applications of chaos theory are discussed, culminating in a chaotic interpretation of quantum mechanics and Theory of Everything. Finally, nonlinear analysis and its significance in various real time data are outlined with suitable examples and illustrations.

Keywords: Solitons, Chaos, Nonlinear Universe

1. Introduction

Owing to the mathematical simplicity in calculations and computations pertaining to linear and well-proportioned systems, the world of science has stayed in a slumber of ignorance for one millennium too many [1-2]. It is only recently that scientists have woken up to the hard reality that linearity is but a tiny part of the bigger nonlinearity that governs the universe [2]. This is evident from two simple facts often seen in nature's behavior. Firstly, no system keeps on exhibiting proportional increase/decrease in output as the input keeps increasing/decreasing; there is at least one point when the system reaches saturation and the changes in output are no longer proportional to the changes in input [3]. Secondly, the world is not all about clockwork precision – there are hundreds of factors, not all of them known apriori, driving the behavior of the system so wildly that it becomes difficult to predict anymore. A classical example of this is the weather [4].

Even since the advent and rather explosive growth in nonlinear studies, one observes a largely mathematics-dominated route, where nonlinear phenomena such as solitons, chaos, fractals and nonlinear analysis are largely dominated by nonlinear differential equations describing their behavior [5]. It is indeed true that the language of mathematics gives life to an otherwise difficult-to-understand behavior of nature that rendered Lorenz and Poincare befuddled in their studies of weather patterns and solar system

mechanics respectively [6-7]. Moreover, such mathematical descriptions and endless papers in literature have enabled one to identify nonlinear phenomena in numerous cases of nature including physics, biology, chemistry, astronomy, engineering and statistics [8].

However, the mathematics dominated research efforts in nonlinear studies may have given rise to the inevitable – we have lost track of the big picture. The very philosophy underlying nonlinearity has been obscured, with the focus entirely on mathematical descriptions and physical applications of nonlinearity.

In this paper, I intend to address this issue. Particularly, the two aspects of nonlinearity – solitons and chaos, are focused on and the generic philosophy underlying the duo is discussed, based on their well known properties. A brief review of the various applications of solitons and chaos is outlined, standing testimony to the ubiquity of the philosophy underlying the duo.

2. Solitons

Perhaps, the simplest way to describe a soliton is as a time/space-varying signal possessing a bell curve shape. Principally, the following types of nonlinear partial differential equations are identified, leading to three kinds of solitons:

1. The Korteweg-de Vries (KdV) equation of the typical form $\partial_t \emptyset + \partial_x{}^3 \emptyset + 6\emptyset\partial_x \emptyset = 0$, with the usual notation for space and time partial derivatives. The corresponding soliton solution is $\emptyset(x,t) = \frac{1}{2} csech^2\left[\frac{\sqrt{c}}{2}(x - ct - a)\right]$. This form has applications in shallow water wave hydrodynamics, plasma and crystal lattice based acoustic waves [9].
2. The Nonlinear Schrodinger equation (NLSE), typically given in classical field theory and optics as $i\partial_t \psi + \frac{1}{2}\partial_x{}^2 \psi + N^2|\psi|^2\psi = 0$, with N denoting the balance between linear dispersive and nonlinear effects, and for N=1, one gets fundamental solitons as $\psi(x,t) = \text{sech}\,(x)e^{it/2}$ [10].
3. The Sine-Gordon (SG) equation, given in real space time coordinates as $\emptyset_{tt} - \emptyset_{xx} + sin\emptyset = 0$, and the corresponding 1-soliton solutions have the form $\emptyset(x,t) = 4arctane^{mu(x-vt)+d}$, where $u^2=1/(1-v^2)$ [11].

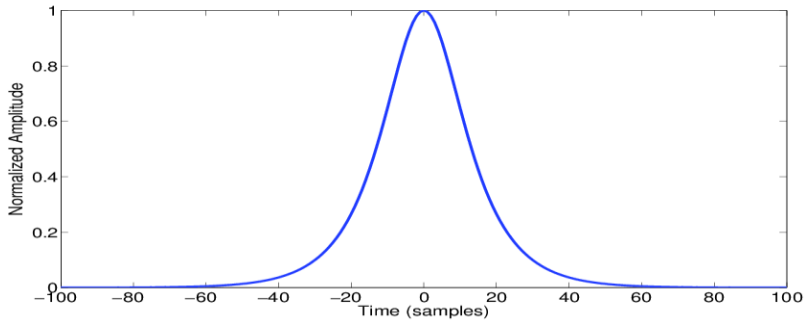

Figure 1 A 1D Hyperbolic Secant Signal

Apart from the above mentioned forms, various other forms of the soliton such as breathers, oscillons, peakons, nematicons, compactons and similaritons exist [10]. An example of a hyperbolic secant based soliton is shown in Fig. 1.

The most immediate observation from Fig. 1, is the bell shaped curve, possessing an exponential rise from 0, reaching to a zenith at the peak, followed by an exponential fall back to zero. This is in stark contrast to the abrupt rise and fall of a rectangular pulse. Also, one observes that the pulse possesses compactness, with non-zero values limited to a very short duration. This 'solitary' nature of the pulse earns it the name 'soliton'.

With a little imagination, it is easy to see that the shape of the soliton depicted in Fig. 1 represents the progress of life. From zero, the signal emerges, signifying birth. Following this, is a period of growth, almost exponential. One observes that the rate of growth initially increases and then decreases, until a zenith is reached. This signifies that growth cannot be permanent, a saturation point will eventually be reached. Following this, one observes a decay, a decline in a manner that mirrors the growth seen earlier. Again, the rate of decay increases initially and then decreases. Finally, the signal vanishes into zero, signifying death. In stark contrast to sinusoidal waves that unrealistically have non-zero values extending towards infinity, (and thus non-compact), the solitons signify a real-life process of birth, growth, decay and death.

A significant property of solitons is the elastic collision observed, where two solitons travelling with different velocities collide, and after colliding retain their original shapes and values [12]. This is illustrated in Fig. 2.

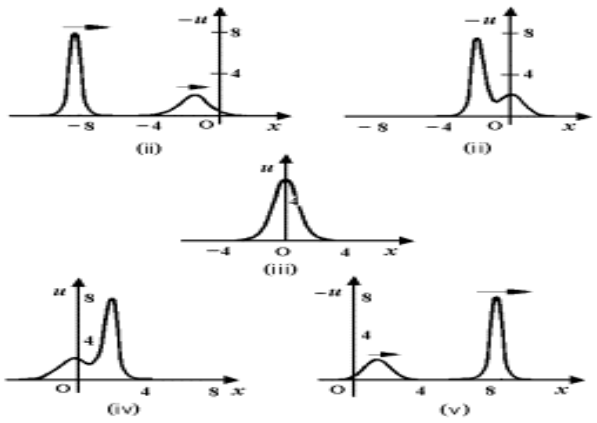

Figure 2 Collision of two solitons

Philosophically, this property demonstrates the resilience of life, in other words, it is possible that when two life-processes interact, each one's values are temporarily and apparently influenced by the other, but such interactions are temporary and in the long-run, the original life-trajectories for each are retained.

Also, solitons represent 'burst' phenomena – a sudden sharp rise from nothingness, back to nothingness. Such a property is commonly seen in hydrodynamics as 'rogue' waves, waves that emerge from nowhere in the far out sea and disappear without leaving a trace [13]. The enormous destruction caused by such waves to ships and ocean liners have caused scientists to study it in detail, giving a plethora of explanations such as thermal expansion, wind waves and modulational instability [13]. However, knowing the hyperbolic secant nature of the soliton, it is possible to generate a spatiotemporal rogue wave, using a spatiotemporal profile given by $C(i+1) = C(i) - \frac{2}{T} tanh\left(\frac{x-D}{T}\right) sech^2\left(\frac{x-D}{T}\right)$, with D and

T denoting the spatial offset and localization factors respectively. A spatiotemporal rogue wave so generated is illustrated in Fig. 3.

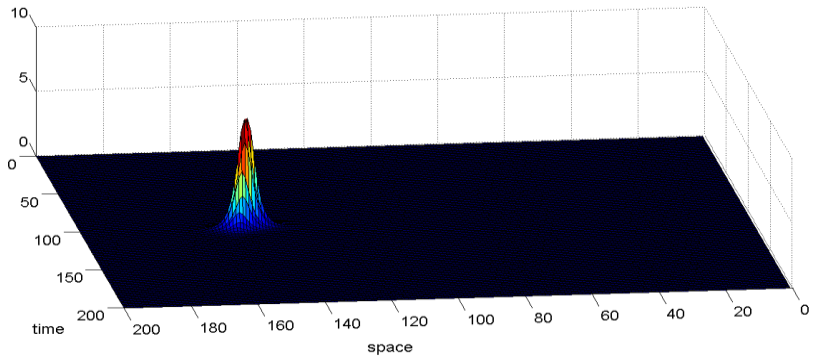

Figure 3 Spatiotemporal Rogue Wave

The burst nature of solitons can be put to good use in another manner. Specifically, certain data in nature, such as tourism data, pulsar waves, Electrocardiogram (ECG) Signals and search trend data possess sporadic looking or periodic bursts. Thus, to analyze such signals for periodicities and discontinuities in a multiscale resolution, one would need to employ compact, smooth, burst-like signal. This is where the 'Solitary Wavelet' comes in handy, where the wavelet is defined by setting the hyperbolic secant function as the scaling function. Figure 4 shows the scaling and wavelet functions of the solitary wavelet.

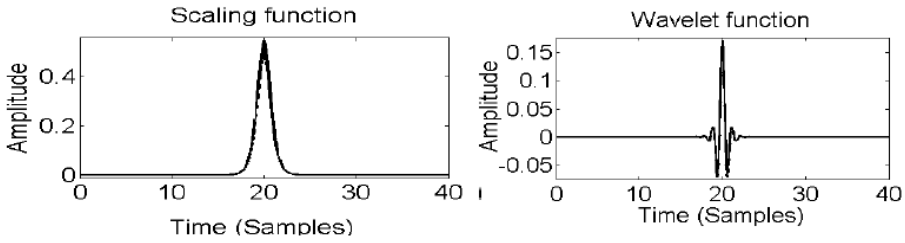

Figure 4 The Solitary Wavelet

The smoothness and compactness of the soliton give rise to a very desirable mathematical feature in the solitary wavelet: the higher order moments of the wavelet function, given by $\int_{-\infty}^{\infty} t^m S(t)dt$, vanish to zero. These moments, upto the tenth order are plotted in Fig. 5 for the solitary wavelet (SOL) on a logarithmic scale, in comparison with the corresponding moments of other wavelets, such as the Daubechies 4 (DB4), Biorthogonal 4.4 (BIOR4.4), Reverse Biorthogonal 4.4 (RBIO4.4), Symlet 4 (SYM4), Coiflets 4 (COIF4) and the Discrete Meyer (DMEY) wavelets [14,15].

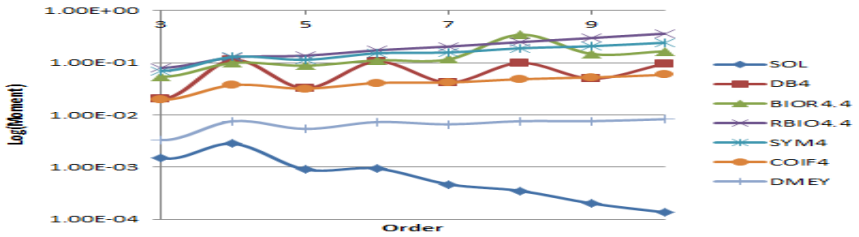

Figure 5 Higher Order Moments of the Solitary and other wavelets

From the plot, one can easily observe the unique negative logarithmic slope for the solitary wavelet alone, which signifies that the higher order moments are rapidly decreasing to zero. This mathematical property translates physically to detection of burst type signals with minimal oscillations, and thus minimal levels of filtering. An example of this property is highlighted in Fig. 6, where an ECG signal is analyzed using both solitary and Daubechies 4 wavelets, and the shift and scale coefficients are plotted.

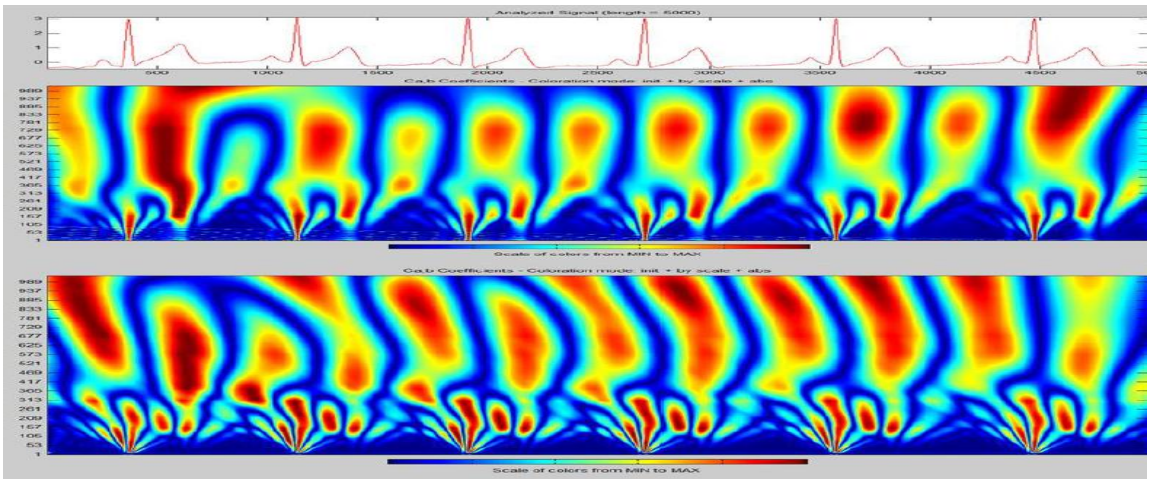

Figure 6 Solitary vs db4 Analysis of ECG Signal

It is seen that while the solitary wavelet exhibits straight-forward peaks corresponding to P, QRS and T waves in the ECG signal, the db4 analysis exhibits various spurious peaks for each peak in the ECG signal data, thus requiring multiple levels of filtering to remove such spurious peaks. Thus, a solitary wavelet analysis of an ECG signal with varying heart rates is shown in Fig. 7, where it is seen that if the scale of analysis is set to correspond to one of the heart rates, the ECG cycles corresponding to other heart rates are significantly attenuated, enabling thresholding and detecting of peaks in the desired heart rate.

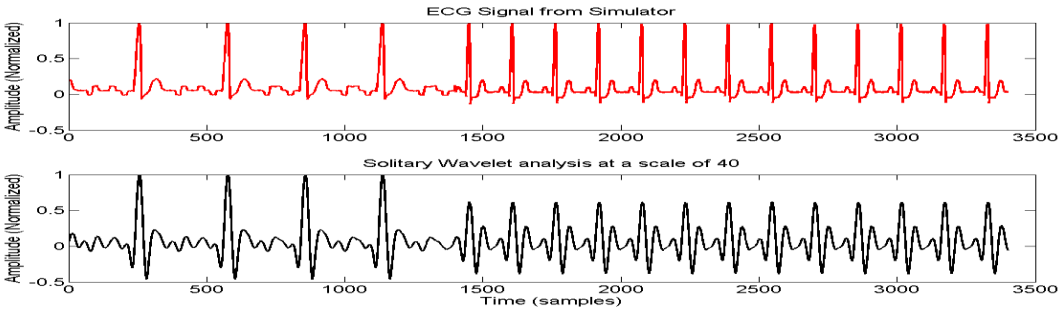

Figure 7 Solitary wavelet analysis of an ECG signal with two different heart rates

Another example of the ubiquity can be seen in the soliton based impulse response signals of most semiconductor devices [16]. As an example, the impulse responses of a PN Junction Diode and an N-Channel Enhancement MOSFET are shown in Fig. 8.

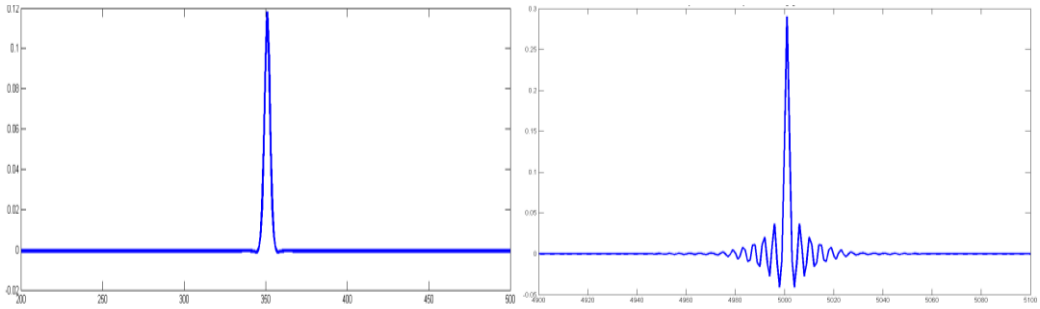

Figure 8 Solitary Impulse responses of PN Junction Diode and MOSFET

The practical application of this property is that solitons can be generated using extremely simple circuitry consisting of a single transistor, where the phenomenon of modulational instability can be used to break a sinusoidal input fed to the input of such a circuit into a train of solitons, by building multiple harmonics around the fundamental frequency [17]. A schematic of an Adaptive Bias Controlled Ring Oscillator (ABCRO) soliton generator using this principle and the output waveform is shown in Fig. 9.

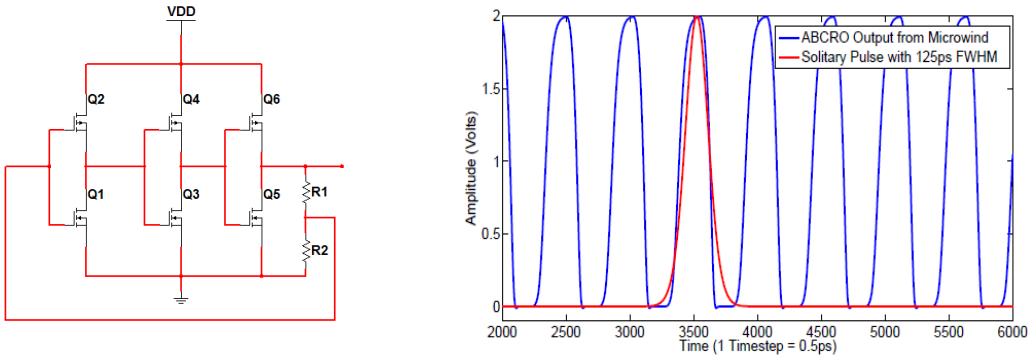

Figure 9 Schematic and Output of ABCRO based Soliton Generator

The solitons thus generated can be used to form a system of Return to Zero Logic, with Fig. 10 illustrating the output waveforms of a Soliton based NAND Gate. Alternatively, it is seen that soliton based transmission exhibits larger ranges in free space optic transmission, tabulated in Fig. 10 for green wavelengths [18].

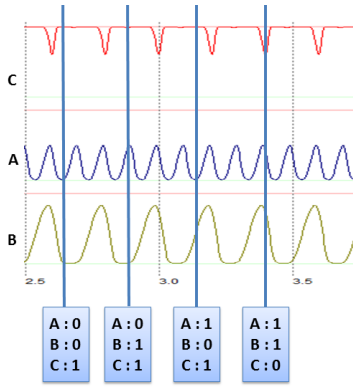

Signal	Distance	Attenuation (dB)
Sine	1 cm	-4.33
	10 cm	-15.67
	15 cm	-14.69
Square	1 cm	-3.95
	10 cm	-13.91
	15 cm	-14.69
Solitons	1 cm	-0.11
	10 cm	-9.19
	15 cm	-10.58

Figure 10 Soliton NAND Gate waveforms; Free Space Optics using Solitons

It is also seen that when conventional square and sine carriers are replaced with soliton carriers in state-of-the-art and futuristic telecommunication systems, the distortion rates are reduced greatly. This is because the spectral profile of a soliton pulse resembles a soliton pulse, implying that solitons have an exponentially decaying spectral profile. Such a profile protects it from high frequency attenuation in low-pass based transmission channels, as well as making it less vulnerable to noise, owing to the compactness of the pulse. Fig. 11 shows the eye diagrams and bit error rate comparisons of a 2 TeraHertz Radio over Fiber Communication System employing Orthogonal Frequency Division Multiple Access (OFDMA) and Amplitude/Phase Shift Keying Modulations using a combined Photonic Crystal Fiber-Microstrip-Wireless Channel [19].

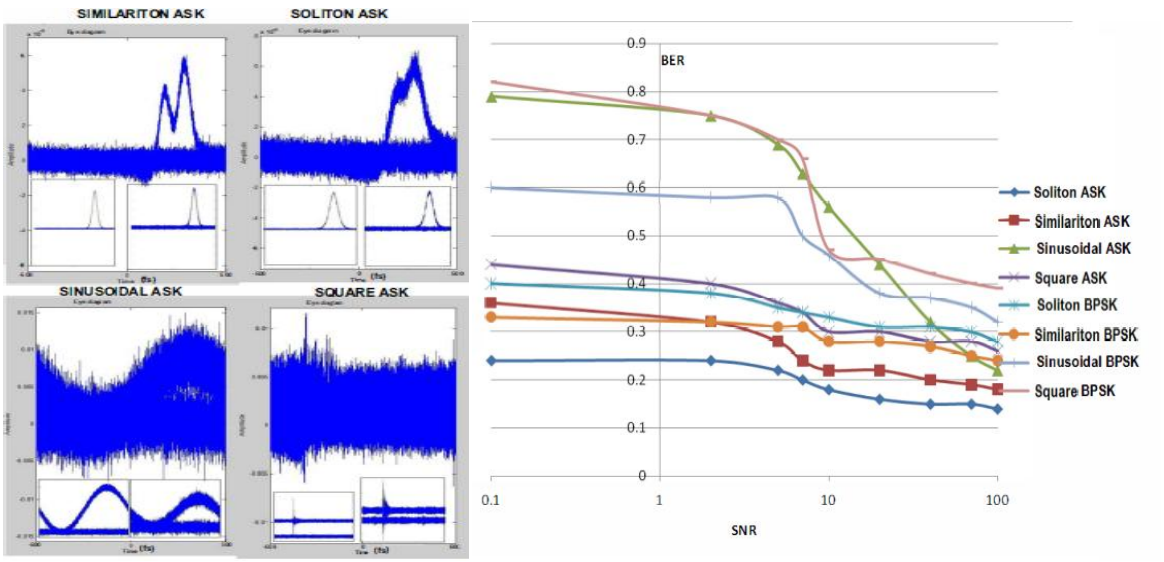

Figure 11 Solitons in THz Radio over Fiber Communications

A Special case of solitons are light-bullets or spatiotemporal solitons, which are localized in 2 spatial and one temporal dimensions [20]. Such solitons are extremely unstable, and are subject of active research in photonics and liquid crystal displays (LCDs) [21-22]. It is seen that using a 'photonic crystal' comprising of silicon rods of 60nm radius on free space background with a lattice unit of 500nm, designing of a line defect with progressively increasing width (taper), it is possible to generate such discrete light bullets, as shown in Fig. 12.

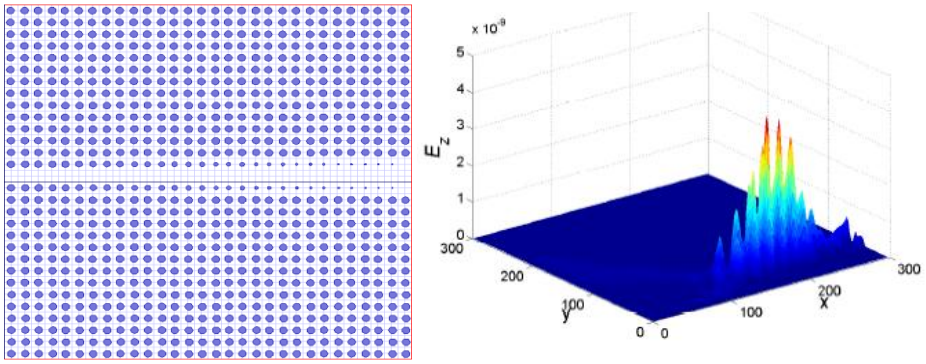

Figure 12 Formation of light bullets in photonic crystals

From the above examples and illustrations, one can easily observe how the life-representative nature of the soliton makes it extremely ubiquitous in various aspects of signal processing, translating into technological advantages of simplicity, low distortion, longer transmission range and effective detection of burst type signals. As a testimony to the ubiquity, the following are some more examples of solitons:

1. A variety of the soliton, namely, the 'dissipative soliton', emerges, when a gain-loss axis balance is added to the familiar dispersion-nonlinearity balance [23]. It is seen that such solitons can be generated by using a phase shifting RC network in the feedback path of a soliton generator. The generated dissipative solitons are seen to resemble the spiking neuron action potential, described by the FitzHugh Nagumo model, a simplified version of the Hodgkin Huxley model illustrating the gated ion channel charge transfer mechanism in nerve cells [23-24].

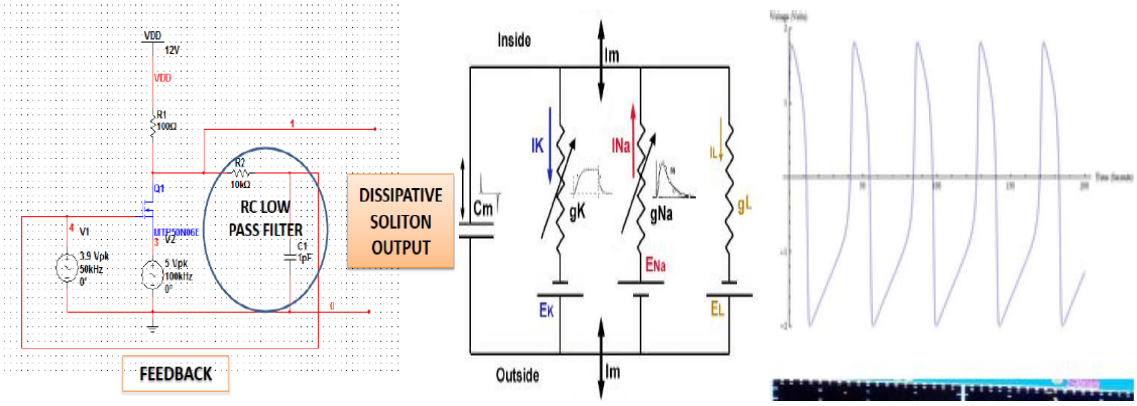

Figure 13 Dissipative Solitons - Generator and the FitzHugh Nagumo model

2. Falaco Solitons are topological phenomena created by macroscopic rotational dynamics in a continuous media with a discontinuity surface, such as a swimming pool [25]. The solitons are "stationary" thermodynamic states far from equilibrium, which are locally unstable but are globally stabilized. It has been conjectured that the universal coherent topological features of the Falaco Solitons can appear as cosmological realizations of Wheeler's wormholes, representing spin pairing mechanisms in the microscopic Fermi surface, and exhibit the confinement of sub microscopic quarks on the end of a string, or realizations of sub-submicroscopic strings connecting branes [25].

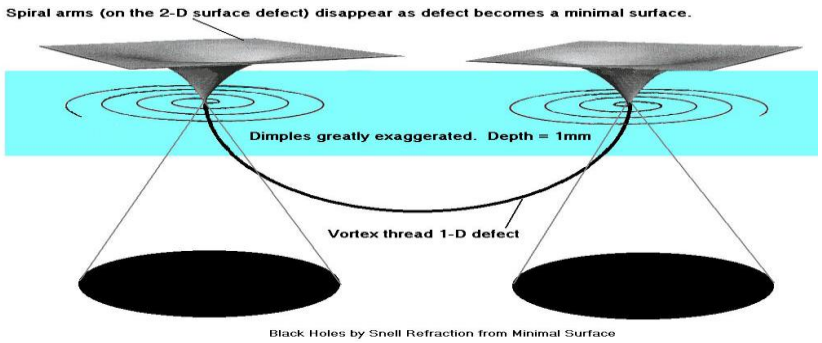

Figure 14 Falaco Solitons

3. Solitons have been found in protein folding mechanisms, DNA reading, Bose-Einstein condensates, tsunamis, scalar hairy black holes and cyclone vortices [26-30].

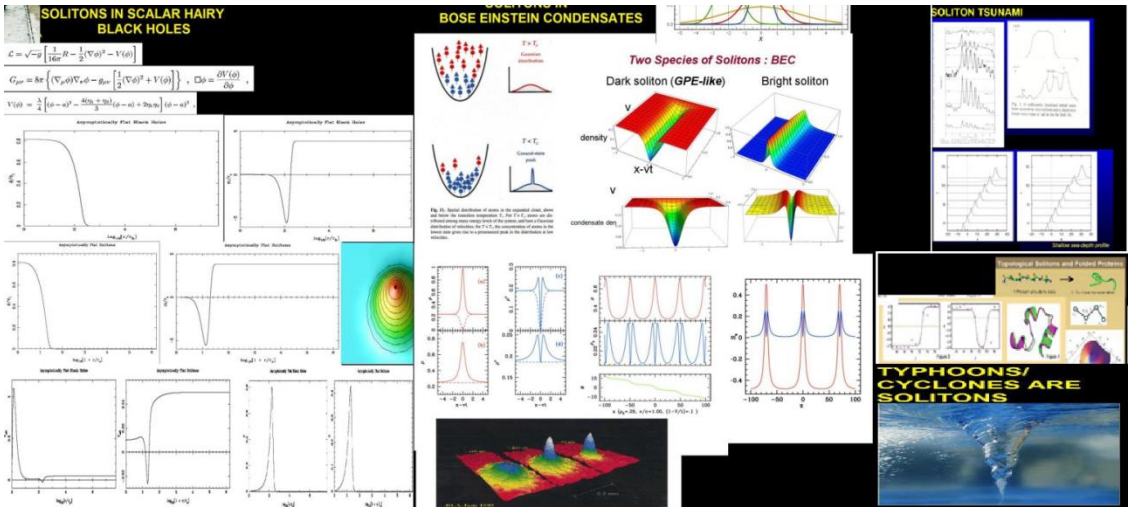

Figure 155 A few phenomena involving solitons

3. Chaos

The most characteristic defining properties of chaos are determinism and an extremely sensitive dependence on initial conditions. By determinism, it is meant that there exist definite mathematical equations by which one can determine the state of a chaotic system at any given time [8]. However, such a system has very sensitive dependence on certain factors, called the initial conditions. In most cases, it is impractical to know with extreme certainty, the values of these initial conditions, and a small error in the initial condition values leads to an inexplicably large error in predicting the output of a chaotic system, rendering it 'theoretically deterministic, yet practically random'. In other words, a Chaotic system is one where the present determines the future, but the approximate present does not approximately determine the future.

The sensitive dependence on initial conditions is popularly known as the "butterfly effect", so-called because of the question posed as title of a paper given by Edward Lorenz: Does the Flap of a Butterfly's Wings in Brazil set off a Tornado in Texas? The flapping wing represents a small change in the initial condition of the system, which causes a chain of events leading to large-scale phenomena [8]. Had the butterfly not flapped its wings, the trajectory of the system might have been vastly different. Thus, two trajectories, separated by an infinitesimally small interval dZ, after a time t, end up as $dZ(t) \approx e^{\lambda t}|dZ|$, with the parameter λ, termed the "Lyapunov Exponent" and computed using the Rosenstein Algorithm, quantifying the sensitivity [31-32].

Perhaps the most famous and simple example of a chaotic system is the logistic map, given by $x_{n+1} = rx_n(1 - x_n)$ [33]. Such an equation, describing the n+1th sample of a system in terms of its nth sample is termed an 'iterative map', and it describes how a system evolves with respect to its previous sample. The parameter 'r', termed the 'control parameter' largely controls the evolution of such a system. A plot of x(n) as a function of r illustrated for what values of r the system exhibits orderly or chaotic behavior and

how it transits from one to the other. Such a plot is termed the bifurcation plot and is as shown in Fig. 16 for the logistic map. It is seen that the value of r=3.56995 signifies the onset of chaos.

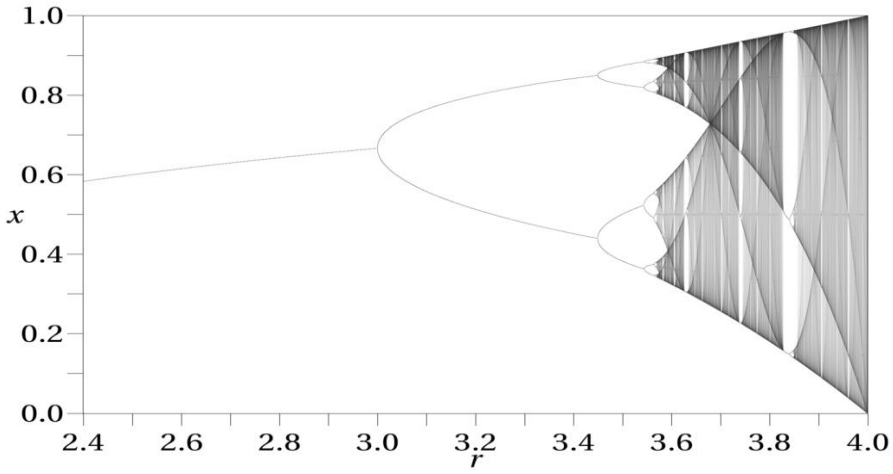

Figure 16 The Logistic Map

Another classic example of chaos is the Lorenz system of attractors, given by the set of coupled equations $x' = S(y - x); y' = x(P - z) - y; z' = xy - Bz$. Here, S, P and B denote the control parameters. This chaotic system is most popular for the butterfly shaped phase plot, termed the 'attractor', and shown in Fig, 17 [34]. From a signal processing perspective, a phase portrait is a plot of a signal C with its derivative C'(t). Such a plot illustrates the phase space dynamics of the system, also highlighting the evolution trajectory of time [8].

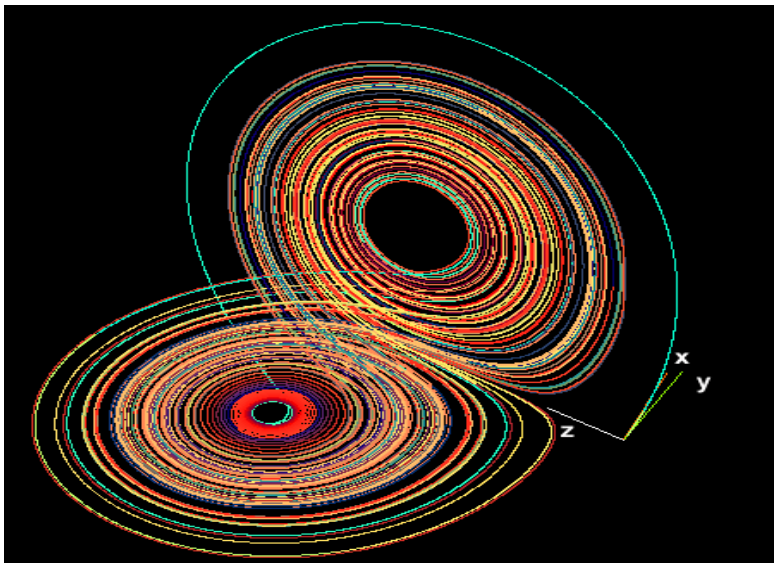

Figure 177 The Lorenz Attractor

Coupled systems such as these are typically implemented using Chua Circuits, consisting of positive feedback amplifier circuits possessing one or more nonlinear negative resistance elements called 'Chua Diodes' [35]. Such elements approximate nonlinearity using piecewise linearity. However, the tenability

of such circuits comes into question at high frequencies when implemented using integrated circuit electronics.

It is for this reason and to expand the scope of chaos generation that one needs to consider a novel kind of chaos, termed 'signal based chaos'. Here, the control parameter is not a system related parameter such as resistance or capacitance; rather it is a signal parameter such as frequency or phase ratio.

In this context, the standard circle map depicts a 'driven' chaotic system, where the chaos is caused by the competing frequencies of two driving signals/oscillations [36]. The standard circle map iterative function is given by $\theta_{n+1} = mod\left(\theta_n + \omega + \frac{K}{2\pi} sin(2\pi\theta_n), 1\right)$. Here $\omega = f_2/f_1$ denotes the ratio between the driving frequencies and acts as the control parameter along with K, where for K>1, noninvertible behavior leading to chaos is observed. By adapting this equation using a few modifications changing the variable from phase to frequency and appropriate normalizations, one obtains the iterative map of a 'Frequency Dependent Chaotic' system, as $f_0(i+1) = mod\left(f_0(i) + \frac{f_2}{f_1} - V(f_0(i)), \pi\right)$, where $r = f_2/f_1$ is the control parameter. The bifurcation map and cobweb plots (plots of x(n+1) as a function of x(n) for a particular value of r) of such a chaotic system is shown in Fig. 18.

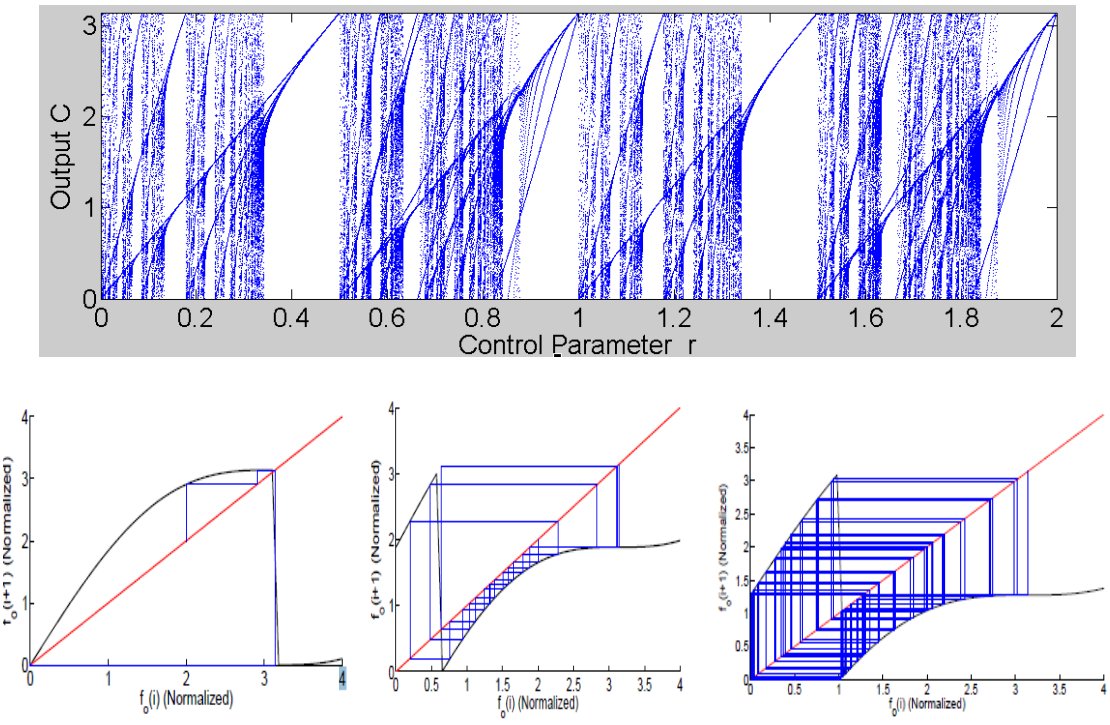

Figure 18 Bifurcation and cobweb plots (r=10; 10.7; 3.4π) for frequency dependent chaos

It is seen from Fig. 18 that while the bifurcation trends are periodic, irrational values of r, such as 3.4π give rise to well-spread and ornamental cobweb plots signifying chaotic behavior.

It is possible to physically realize this chaotic system using a single CMOS inverter driven by a sum of two sinusoid inputs. The schematic, phase portrait for irrational r and corresponding spectrum are shown in Fig. 19.

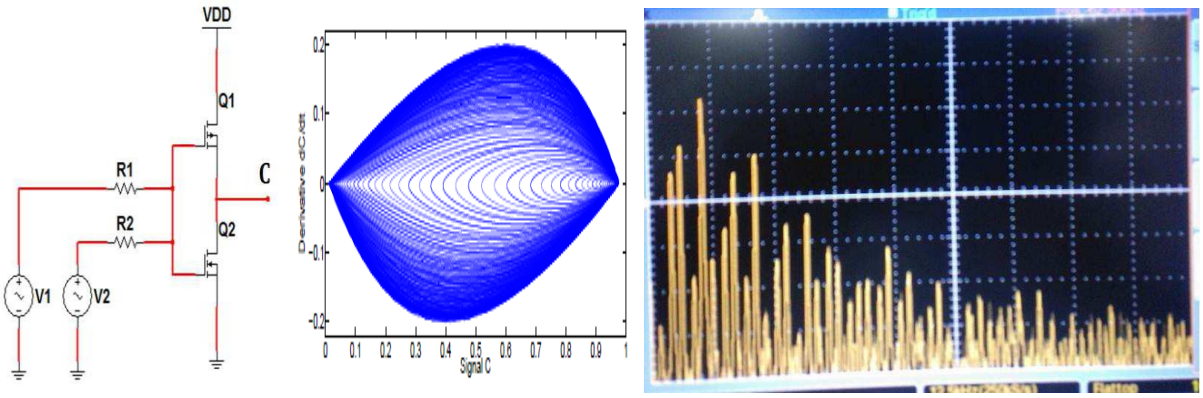

Figure 19 Frequency dependent chaos using single CMOS inverter

While the control parameter is frequency ratio as outlined above, the chaotic parameters for the frequency dependent chaotic system are the output amplitudes and frequencies. The iterative map presented earlier gives the frequency perspective of chaos. Similarly, an amplitude perspective of chaos can be obtained using the iterative map and bifurcation plots, as shown in Fig. 20 for low amplitude case.

$$C_{n+1} = C_n - \frac{51.1766[2A\pi f_1 cos(2\pi f_1 t) + 2Ar\pi f_1 cos(2\pi r f_1 t)]10^{23.0414(Asin(2\pi f_1 t)+Asin(2\pi r f_1 t)-0.3965)}}{1+10^{23.0414(Asin(2\pi f_1 t)+Asin(2\pi f_1 rt)-0.3965^2}}$$

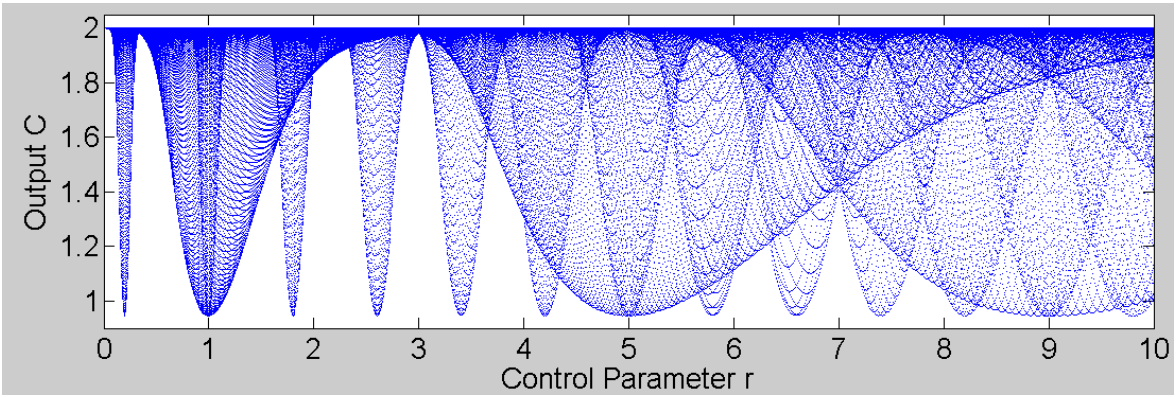

Figure 20 Amplitude perspective of Frequency dependent chaos

One direct advantage of the frequency dependent chaotic system is that it can directly be used for secure communication and computing purposes, with the control parameter r acting as a secure key [37]. To demonstrate this, a secure data embedding system in images is proposed, where the data to be embedded is first modulated using frequency dependent chaos, before additively embedding into the image. The block diagram, phase portraits and the carrier and embedded images are illustrated in Fig. 21. The Peak Signal to Noise Ratio (PSNR) obtained using this technique is quite high of the order of 50-60dB.

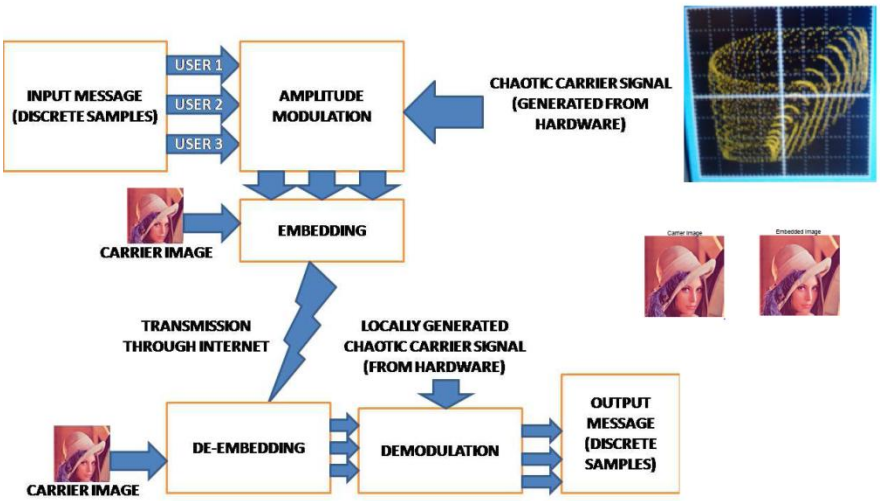

Figure 21 Embedding Data in images securely using frequency dependent chaos

On similar lines, by reshaping the output chaotic signal and embedding an input file, represented as a stream of bytes into it and saving the resultant as a jpg image, it is seen that one is able to compress the input file by a compression ratio of around 5:1-7:1 [38]. This is seen to apply for various filetypes such as txt, pdf, png, 3gp, mp3 and rar.

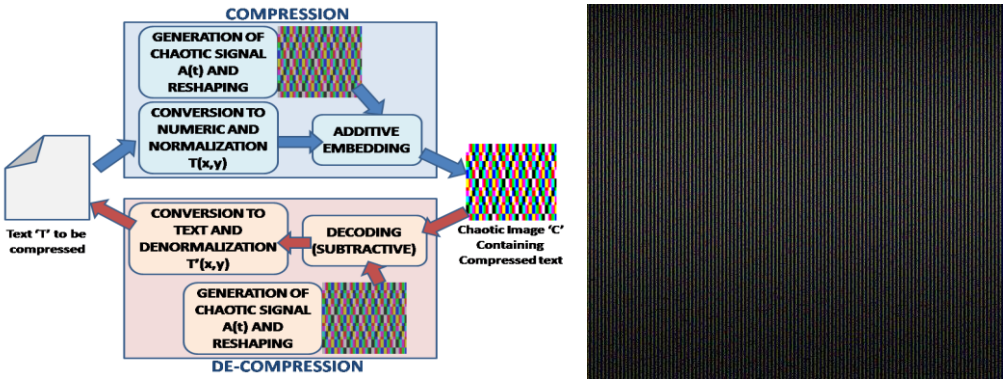

Figure 22 Compression algorithm; Compressed image containing the entire text of 'Gulliver's Travels'

The security obtained by using frequency dependent chaos is characterized by a high value of Mean Square Error of 60% obtained when the control parameter is missed even by a factor of 1% in the receiving end. Since the output file (jpg image) can be viewed as a series of bytes, it is possible to iteratively repeat the compression algorithm, thereby compressing the compressed file even further. Repeated use of the compression algorithm for over 10 iterations is seen to compress a 28.8MB file into final jpg image of 691 bytes, thus achieving an enormous compression ratio of 41750:1. This process is termed 'supercompression'.

By combining the principle of frequency dependent chaos with ABCRO's and solitary wavelets described earlier, it is possible to create Chaotic Solitary Wavelets, which promise apart from compactness and burst detection, the added advantage of security, enabled by the presence of chaos, where the control parameter r acts as a secure key. The schematic, phase portrait and chaotic solitary wavelet functions are shown in Fig. 23.

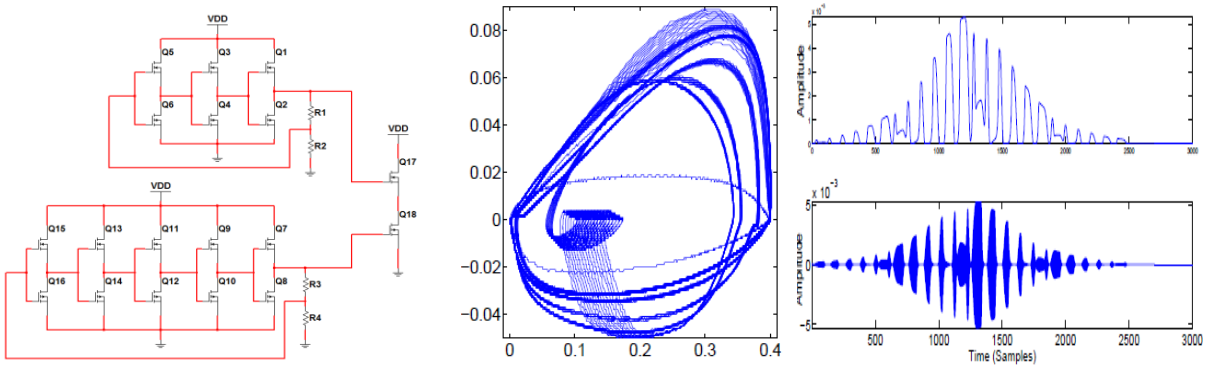

Figure 23 Chaotic Solitary Wavelets

In a similar fashion, it is possible to control a microwave X-band signal, emergent from a Gunn Diode based source, using a low frequency sinusoidal signal, in a master-slave configuration, with chaos observed in the output envelope signal [39]. The schematic, spectra and bit error rates obtained by replacing the Fourier Transform FFT blocks by the Secure Solitary Wavelet blocks in a QPSK-OFDM system are highlighted.

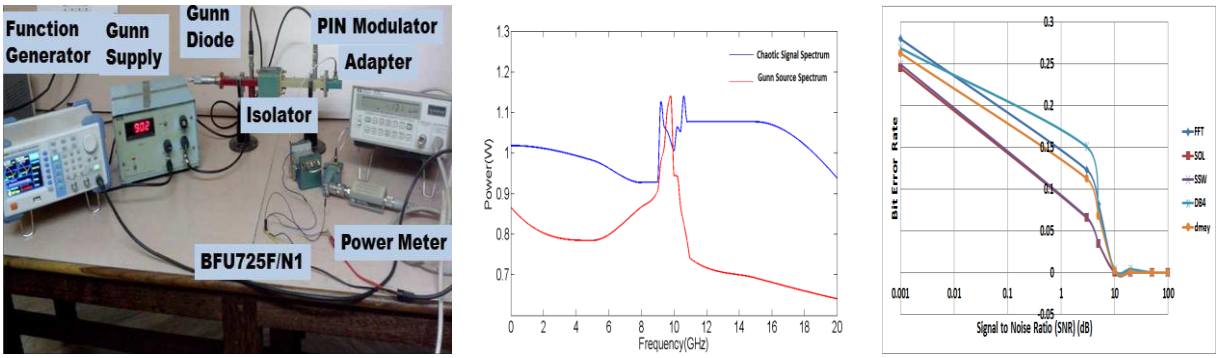

Figure 24a Secure Solitary Wavelets in the microwave X-band range

Generation of Frequency dependent chaos in the X band can also be achieved by coupling two klystron sources onto two arms of a magic tee. By taking output from the third port and terminating the fourth, chaotic output can be obtained. The schematic and input/output waveforms of such a generator are shown.

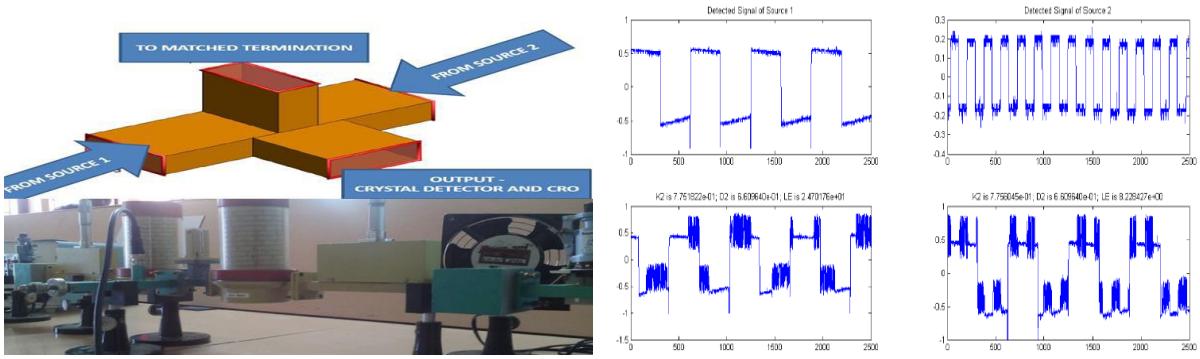

Figure 25b Microwave X band chaos generation using magic tee

The frequency dependent chaotic output of a single transistor circuit, when coupled with a sinusoidal source to a second transistor, produces a novel phenomenon, electrical chirping, where the output frequencies are clearly segregated between the leading and trailing edges.

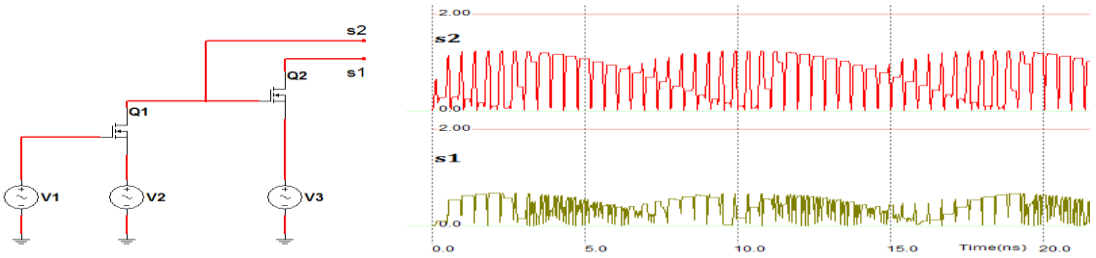

Figure 26 Electrical Chirping induced by Frequency dependent Chaos

Using the obtained chirped signal as the scaling function, one obtains a 'Solitary Chirplet', which is seen to be effective in detecting signals with sudden changes and discontinuities in frequency. As a result, this comes in handy to analyze seismic signals of earthquakes, as shown.

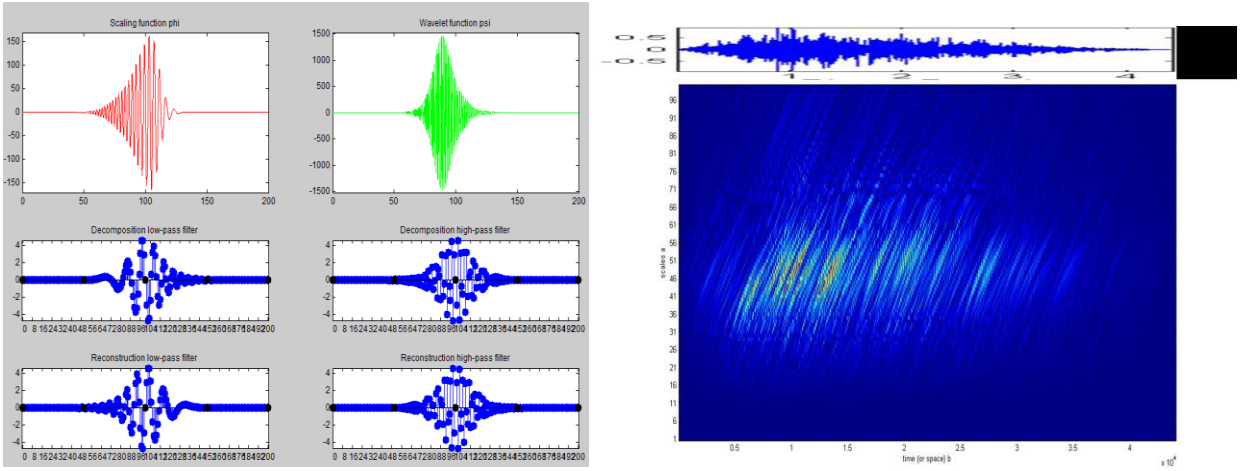

Figure 27 Solitary Chirplet functions and filters; analysis of earthquake signal

A key feature of nonlinearity, often associated with chaotic signals, is the property of 'self-similarity' or fractality [40]. In short, this property ensures that every part of the whole resembles the whole. Fractal structures are found in nature, such as in fern fronds and coastlines. The fractal dimension computed usig the Minkowski Bouligand box counting method is a measure of the self-similarity. One of the most common examples of fractals, shown, is the Mandelbrot set, the set of values of c in the complex plane for which the orbit of 0 under iteration of the complex quadratic polynomial $z_{n+1} = {z_n}^2 + c$, remains bounded [41].

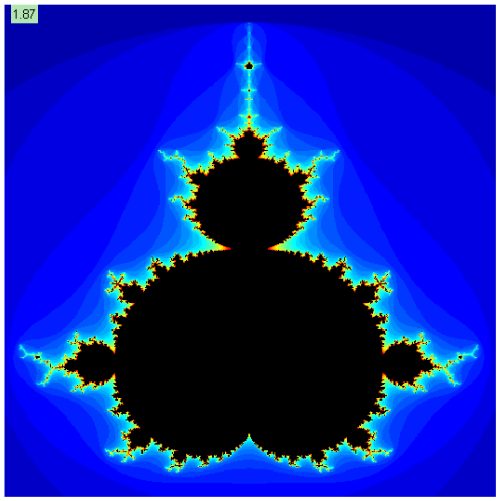

Figure 28 The Mandelbrot Set

It is possible to construct a 1 dimensional chaotic signal from a fractal spectral profile defined using the relation $C(f) = \sum_{i=1}^{N} \frac{1}{i}\delta\left(f - \frac{1}{r^i}\right) + \frac{1}{i}\delta\left(f + L - \frac{1}{r^i}\right)$, where L is the length of the spectral profile and N is the number of iterations. The generated spectral profile and signal, along with the phase portrait and recurrence plot (a plot of the 'recurrence' matrix R(i,j)=||x(i)-x(j)||<T) is shown for r=2.

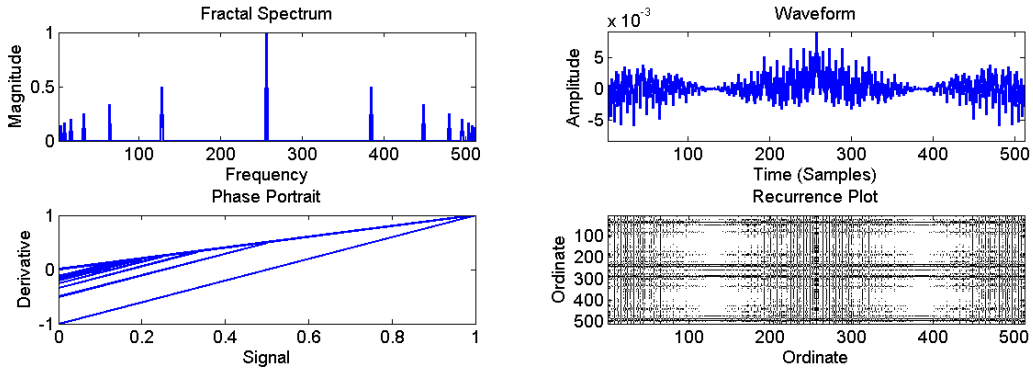

Figure 29 Fractal Chaotic Signal for r=2

A positive Lyapunov exponent of 9.6205 obtained asserts the chaotic nature of the generated signal.

Apart from the single transistor/CMOS inverter based chaos generation, various other methods, primarily using special mathematical functions, exist for generating signal based chaos. Some of these are briefly highlighted below:

A. The Ramanujan Theta Function, given by $f(a,b) = \sum_{n=-\infty}^{\infty} a^{n(n+1)/2} b^{n(n-1)/2}$, is used to generate frequency dependent chaos by setting a and b to sinusoidal signals with frequencies f1 and f2 respectively [42]. The obtained phase portraits for r=2.0322 corresponding to Lyapunov Exponent of 3.36 are shown.

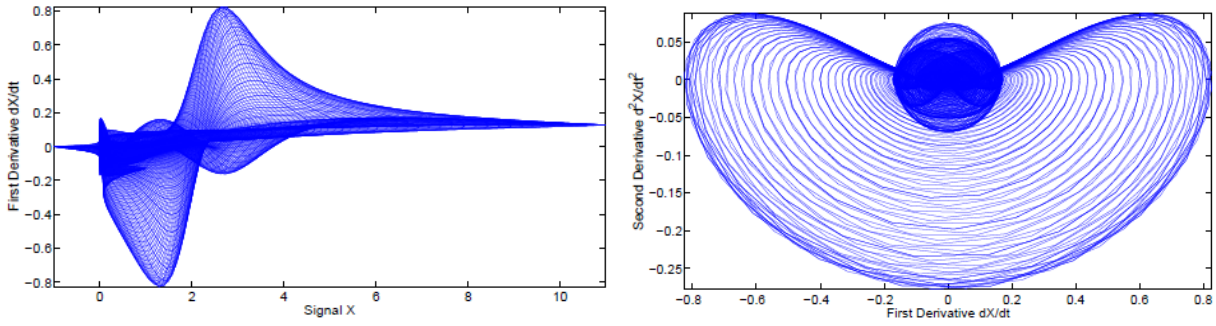

Figure 30 Frequency Dependent Chaos Generation using Ramanujan Theta Functions

B. In a similar manner, chaos is generated using three of the seven third order mock theta functions [43], $\phi(q) = \sum_{n=0}^{\infty} \frac{q^{n^2}}{\prod_{i=1}^{N} 1+q^{2i}}$; $\chi(q) = \sum_{n=0}^{\infty} \frac{q^{n^2}}{\prod_{i=1}^{N} 1-q^{i}+q^{2i}}$ and $\rho(q) = \sum_{n=0}^{\infty} \frac{q^{2n(n+1)}}{\prod_{i=1}^{N} 1+q^{2i+1}+q^{4i+2}}$. In each case, q is replaced with a sum of two sinusoids, and by finding X'(t) for each of the functions represented as X(t), one obtains the iterative map as X(i+1)=X(i)+X'(i). The corresponding phase portraits for r=π are shown in Fig. 3 with Lyapunov exponents obtained as 0.75, 0.53 and 0.63 respectively.

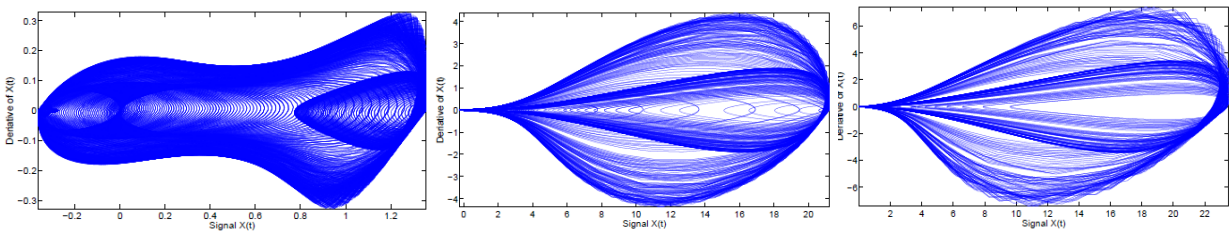

Figure 31 Frequency Dependent Chaos Generation using mock Theta Functions

C. The Ramanujan's Ternary Quadratic Form (RTQF), given as $S = x^2 + y^2 + z^2$ is used to generate chaos by successively iterating each of the three variables x, y and z from 1 to N in nested loop, effectively forming a time series using the form [44]. Also, the nature of generated chaos changes by changing the coefficients of x,y and z in the RTQF from (1,1,1) to Pythagorean (3,4,5), Phi-Pi (1,ϕ,π) and OEN (1,8,9) forms, and by changing the exponents of x,y and z from square (2) to cube (3). The obtained chaotic properties are tabulated.

Basic Form	K (bits/sym)	D	LLE
RTQF-2	7.8552	0.9037	2.3514
RTQF-3	7.7144	0.9037	2.9020
Phi-Pi-2	7.9667	0.9037	2.8060
Phi-Pi-3	7.8731	0.9037	2.6972
Pythagorean-2	7.9880	0.9037	2.5289
Pythagorean-3	7.9037	0.9037	2.3989
OEN-2	7.9467	0.9037	2.3169
OEN-3	7.8413	0.9037	3.1357

Figure 32 Frequency Dependent Chaos Generation using Ramanujan Ternary Quadratic Forms

D. The Bessel functions, which are the canonical solutions of $x^2 y_{xx} + x y_x + (x^2 - n^2) y = 0$ are used to generate frequency dependent chaos by setting x to a sum of two sinusoids of frequencies

f1 and f2 [45]. In particular the form $I_n(x) = \lim_{a\to n} \sum_{m=0}^{\infty} \frac{(x/2)^{2m+a}}{m!\Gamma(m+a+1)}$ gives rise to the bifurcation plots and Lyapunov exponents as shown for the first four orders (n=1,2,3,4).

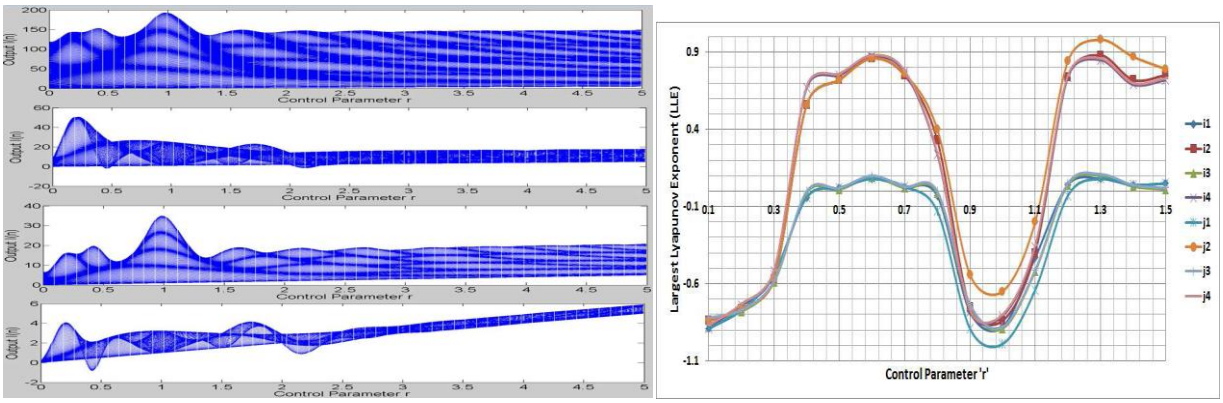

Figure 33 Frequency Dependent Chaos Generation using Bessel Functions

E. Similarly, the Einstein Functions, $E_1(x) = \frac{x^2 e^x}{(e^x-1)^2}$; $E_2(x) = \frac{x}{e^x-1}$; $E_3(x) = \ln(1-e^{-x})$ are used to generate chaos, with bifurcation diagrams as obtained [46].

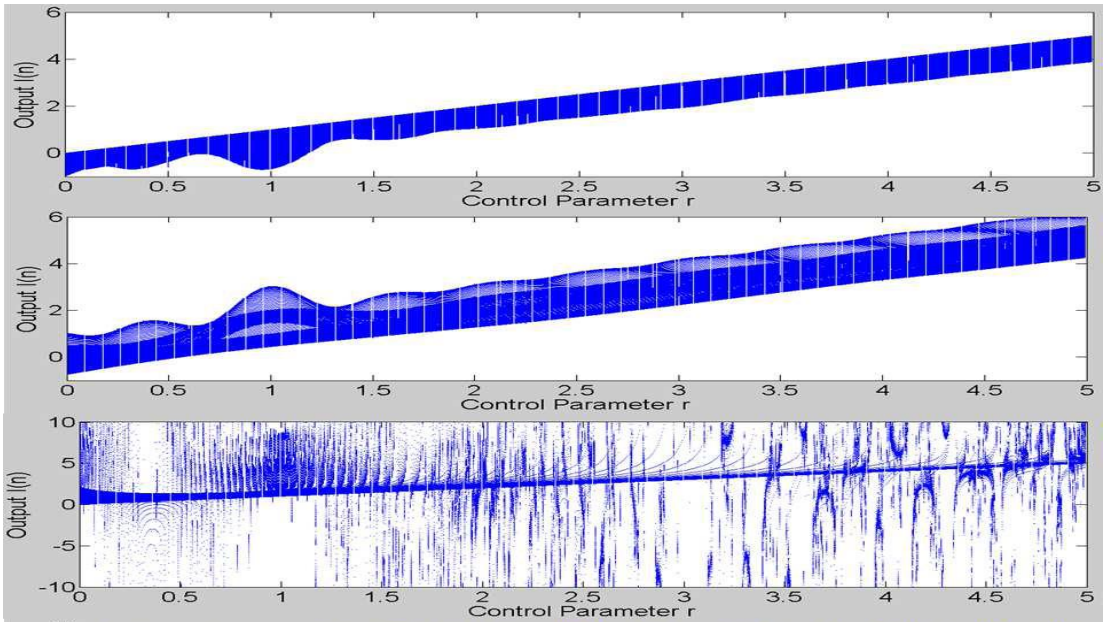

Figure 34 Frequency Dependent Chaos Generation using Einstein Functions

F. The curves, $x(q) = 16sin^3(q); y(q) = 13\cos(q) - 5\cos(2q) - 2\cos(3q) - \cos(4q)$, known popularly as the cardoid curves due to the heart shaped formation [47], can be used to generate chaos, with the obtained phase portraits for r=π.

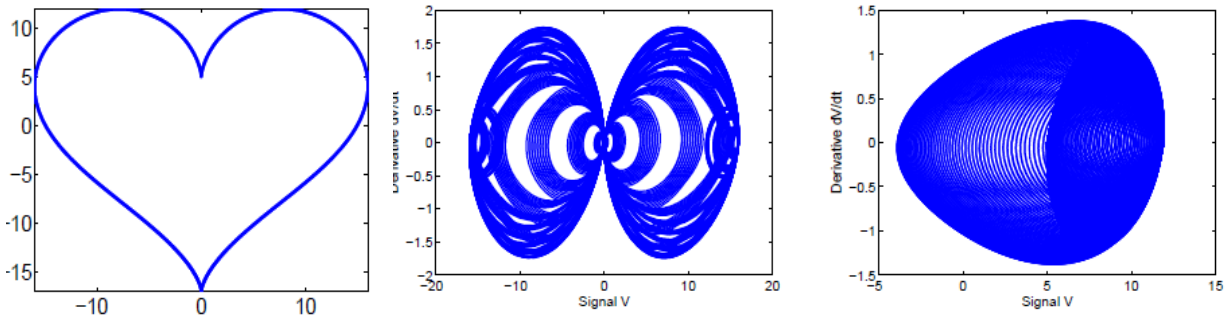

Figure 35 Frequency Dependent Chaos Generation using Cardoid curves

While all the above mentioned illustrations describe temporal chaotic signals, it is possible to extend the concept to generate spatiotemporal patterns using frequency dependent chaos using FPGAs [48]. Specifically, a temporal rule defined by $C(t) = mod(abs[square(f_1 t) - square(f_2 t)], \pi)$ and a spatial rule given by $C(i) = mod(abs[C(i-1) - C(i-1-Nfactor)], \pi)$, generates the following spatiotemporal patterns for various values of Nfactors.

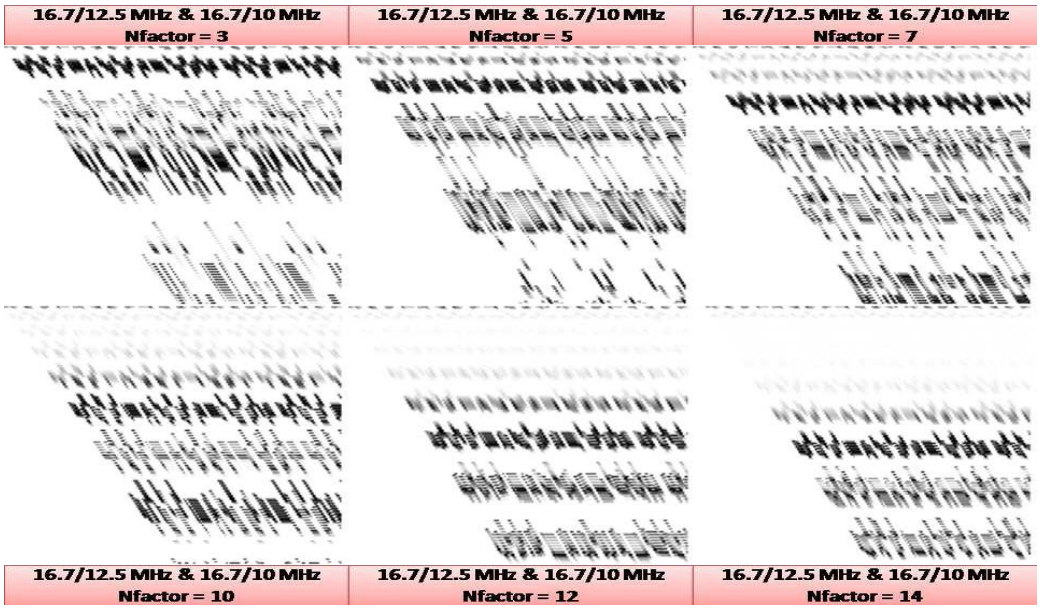

Figure 36 Spatiotemporal patterns using frequency dependent chaos

It is seen that among other phenomena, the generated spatiotemporal patterns exhibit pulse compression, grouping of pulses into triads, regeneration of signals from nothingness, reminiscent of the 'cocoon' stage of a butterfly. Thus, this pattern corresponds to a case of "tunable evolution and emergence". The presence of chaos is characterized by a high value of Kolmogorov Sinai Entropy, which is a measure of the information content carried in the signal [49].

From the above examples and illustrations, one clearly discerns the philosophy behind the principle of frequency dependent chaos, and the ease of tunability obtained by using a signal based control parameter. One also observes how this can be put to use in varied applications.

The phenomena of competing frequencies and exponentially diverging trajectories can easily be translated to the digital logic domain, by the use of square waves of appropriate duty cycles coupled to XOR gates. The resultant is the generation of "Digital Chaos", shown for 3 square waves of 26.79MHz;50%, 9MHz;66.67% and 3.857MHz;70% coupled to 2 XOR gates.

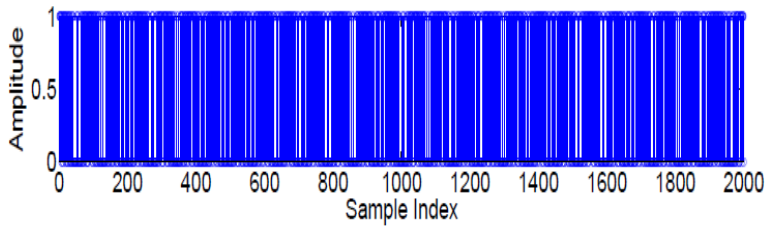

Statistical Test	P-Value	Proportion	Result
Runs	0.1227	0.9910	Pass
Longest Run	0.2343	0.9930	Pass
Monobit	0.1894	0.9890	Pass
Rank	0.2048	0.9940	Pass
FFT	0.8634	0.9940	Pass
Block Frequency	0.4632	0.9910	Pass
Cumulative Sum	0.2011	0.9900	Pass
Nonperiodic Template	0.0352	0.9880	Pass
Overlapping Template	0.3032	0.9920	Pass
Random Excursions	0.1823	0.9940	Pass
Serial	0.1030	0.9860	Pass
Maurer's Universal	0.3973	0.9910	Pass

Figure 37 Generated Digital Chaotic Output

It is seen that the generated output sequence serves as a random number sequence, passing various randomness tests of the NIST standard Test suite [50].

The pseudorandom bit sequence mentioned above is put into good use in devising an algorithm to securely compress DNA Genome sequences, in a similar fashion as described earlier. Compression ratios between 2.5 to 3.5 are observed for DNA sequences such as Escherichia Coli, Streptomycces yeast and the Hepatitis B virus [51].

Philosophically, the inherent 'practical randomness' in the chaotic output as witnessed in the above results can be put to good use in achieving the inherent uncertainty and randomness characteristic of quantum computation systems [52]. Thus, a pseudorandom number generator as outlined above, generating from the set [0,0.5,1] can be used as a qubit (or quantum bit) generator, where 0, 0.5 and 1 correspond to the states of |0>, $\frac{1}{\sqrt{2}}(|0>+|1>)$ and |1> respectively. Termed 'QTrick Bits', the Pauli Rotation, Hadamard and CNOT gates can be implemented as X=1-Q, Z=-Q, Y=ZX/i, H=-0.5[Q-1] and CNOT=QC-QT. These gates are then used to implement a 1 bit Quantum Teleportation using QTrick bits, and the results are shown.

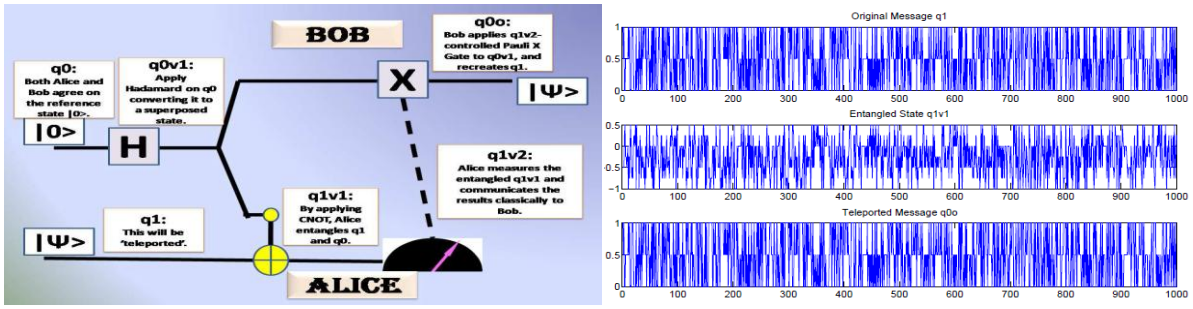

Figure 38 Quantum Teleportation using QTrick bits

It is seen that the QTrick bits are able to successfully implement teleportation with negligible distortion. Furthermore, it is seen that the Lyapunov exponents of the qubits before and after entanglement are observed as 0.7304 and 1.2234, where it is seen that entanglement increases the degree of chaos in the signal. In a similar fashion Quantum Trick Cellular Automata is implemented using QTrick bits [53-54]. Cellular Automata are discrete models studied in computability theory, mathematics, physics, complexity

science, theoretical biology and microstructure modeling. A cellular automaton consists of a regular grid of cells, each in one of a finite number of states, such as on and off. The grid can be in any finite number of dimensions. For each cell, a set of cells called its neighborhood is defined relative to the specified cell. An initial state (time t = 0) is selected by assigning a state for each cell. A new generation is created (advancing t by 1), according to some fixed rule that determines the new state of each cell in terms of the current state of the cell and the states of the cells in its neighborhood.

In the proposed design, each cell is allowed superposed values of 0.5 in addition to 0 and 1, and rules are defined by the operations between a cell y(n) and y(n-1), and the resultant and y(n+1). As an example, the patterns obtained for 1D Quantum Trick Cellular Automata for CNOT/Entanglement and Entanglement/CNOT gate combinations are shown.

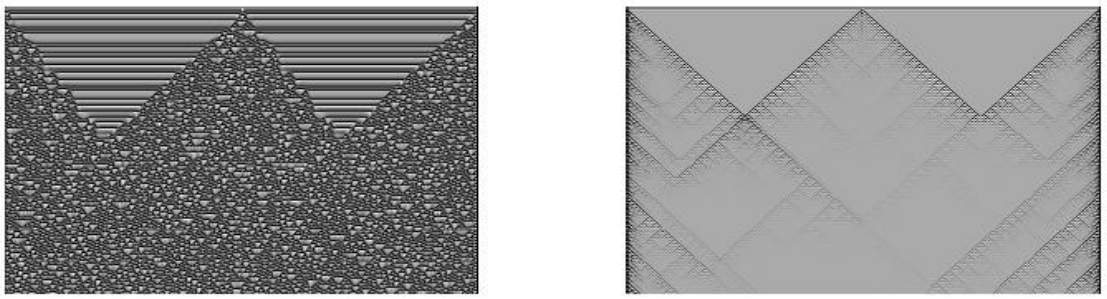

Figure 39 Quantum Trick Cellular Automata for CNOT/Entanglement and Entanglement/CNOT Rules

The ability to perform quantum teleportation using QTrick bits, and by extension, using chaos, forms the motivation in introducing a Chaos Theory based interpretation of Quantum Mechanics [55-56]. The rationale here is that chaotic signals are rich in information, as identified by the high values of Kolmogorov Entropy, a property shared with qubits. The postulates of Quantum Mechanic interpretation using chaos theory then are as follows:

1. The superposed state of a quantum system, depicted by its wavefunction ψ is seen as a chaotic signal.
2. Quantum mechanical collapse, resulting in superposed state 0.5 going back to classical states 0 or 1, is seen as a stage in the evolution of ψ, characterized by a reduction in chaoticity and asymmetry.
3. The extremely sensitive dependence on initial conditions property of chaos renders the system practically random.
4. Collapse is related to measurement operation, and is an irreversible process.
5. Measurement and initial configurations together form the initial conditions of the system.
6. Measurement only determines "when the system will collapse" and not "what the system will collapse to".
7. Using these points, one writes the Schrodinger Equation as $i\hbar\frac{\partial\psi(t)}{\partial t} = H[\psi(t)] = E.\psi(t)$ [56].

A schematic illustrating the chaotic interpretation of quantum mechanics along with the comparison with other existing interpretations is shown [55-56].

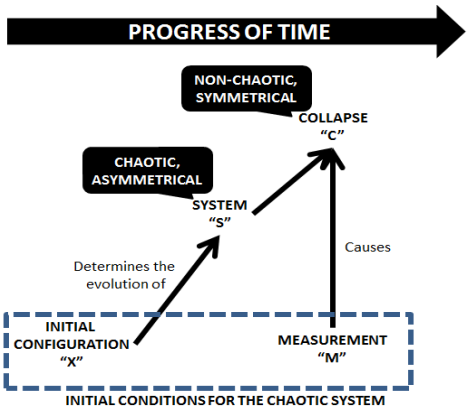

Interpretation	Determinism	Real	Unique History	Hidden Variable	Collapse	Observer Role	Local	CFD	Universal ψ
Ensemble	Agn	No	Yes	Agn	No	No	Agn	No	No
Hydrodynamic	Yes	Yes	Yes	Yes	No	No	No	Yes	Yes
Copenhagen	No	No	Yes	No	Yes	Causal	Agn	No	No
Broglie-Bohm	Yes	Yes	Yes	Yes	No	No	No	Yes	Yes
Von Neuman	No	Yes	Yes	No	Yes	Causal	No	No	Yes
Q – Logic	Agn	Agn	Yes	No	No	Interpret	Agn	No	No
T Symmetric	Yes	Yes	Yes	Yes	No	No	Yes	No	Yes
Many Worlds	Yes	Yes	No	No	No	No	Yes	No	Yes
Popper	No	Yes	Yes	Yes	No	No	Yes	Yes	No
Stochastic	No	No	Yes	Yes	No	No	No	Pos	No
Many Minds	Yes	Yes	No	No	No	Interpret	Yes	No	No
Consistent H	Agn	Agn	No	No	No	Interpret	Yes	No	No
Obj Collapse	No	Yes	Yes	No	Ye	No	No	No	No
Transactional	No	Yes	Yes	No	Yes	No	No	Yes	No
Relational	Agn	No	Agn	No	Yes	Intrinsic	Yes	No	No
Chaotic	**Yes**	**Yes**	**Yes**	**No**	**Yes**	**Timing**	**No**	**Yes**	**Yes**

Figure 40 Interpreting Quantum Mechanics using Chaos Theory

It is seen that while equating uncertainty of quantum mechanics with the practical randomness of chaos theory, the above mentioned interpretation can be used in conjunction with the computational universe model, which equates the action of computational 'matter' (defined by the angle of phase shift (scattering) that a qubit undergoes on passing through each quantum gate), and the action of gravitation of spacetime geometry, according to the Einstein Regge Equations $\sum_h \frac{\delta A_h}{\delta g_{ab}} g_{ab}(l) = 16\pi G U \Delta V_l = 16\pi\hbar G\theta_l$ [57]. This concept, along with the principle of metahomeomorphism, which states that all n-dimensional informational fields are equivalent in information space, leads to three important results:

1. By rewriting the Friedmann-Robertson-Walker (FRW) equations for an approximately homogenous, isotropic universe as $H' = -\frac{16\pi GK}{3}$; $\frac{8\pi G(K+U)}{3} = H^2 - \frac{k}{a^2}$, with k=0 for zero curvature, Hubble parameter H=a'/a, potential energy U=ħθ/ΔV, it is possible to define the computational universe in terms of three regions of Kinetic Energy K: K>3U corresponding to ordinary matter dominated universe, U<K<3U corresponding to dark matter with non-inflating negative pressure (p=K/3–U) and K<U corresponding to dark energy undergoing inflation [57].
2. It is seen that the entangled state of a qubit possesses high degree of chaos, highly asymmetric and characterized by a high mass according to the computational information paradigm. Thus, a 3 qubit entangled state, the GHZ state is equated to an STU black hole given by Reissner Nordstrom line element as a solution to the Einstein Maxwell theory [58]. The entropy of the black hole is given as S=π√|ABC|, with ABC defined as a 3D hypermatrix corresponding to the GHZ state.
3. The E8 Theory of Everything unifies the fields of gravity and the standard model as an E8 principal bundle connection, illustrated, composed of a SU(3) for the strong nuclear force, SU(2)xU(1) for the electroweak, SO(3,1) for the gravitational force along with the frame Higgs and three generations of Fermions, with all the ensuing interactions and dynamics described by curvature and action over a 4D base manifold [59]. The crux of this theory is the development of eight quantum numbers which together, identify each of the 240 roots of the E8 polytope as a fundamental particle. Thus, in essence, the intricate interaction of the beautiful E8 with the fabric of spacetime crystallize into 8 kinds of charges in the charge space. These 8 charges are defined for every point in spacetime, since the E8 is present in every point of spacetime. From basic definitions, it is known that any function (in this case, charge) varying with space and time is a

"signal". So, the 8 charges are seen as 8 signals - signals of information. Using the Chaotic Interpretation, the superposed state of a quantum system, such as a qubit, is nothing but a chaotic signal. The chaotic nature is destroyed once the qubit collapses to a 0 or 1. The initial conditions already determine which of the 2 options (0 or 1) the qubit will collapse into, once we 'measure' it. For a 2 qubit system, represented by 2 chaotic signals with entanglement, there are 4 main states (00,01,10,11) and any entangled state can be formed by combining the 4 states in suitable proportions. Similarly, 3 chaotic signals, representing 3 qubits can have 8 fundamental states (000,001,010,011,100,101,110,111) using which entangled states can be constructed. Thus, given 8 columns of data, according to metahomeomorphism, one can represent them as the combining factors of the 8 states, and represent these 8 states as entangled states of a 3-qubit system. According to the chaotic interpretation, the 3 Qubits are 3 chaotic signals representing – information, represented as the 8 states.

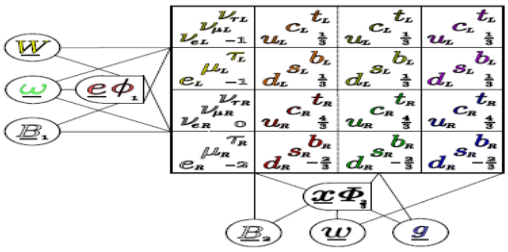

Figure 41 Periodic Table of the E8 ToE

4. Nonlinear Analysis

In the previous sections, the principles underlying solitons and chaos were elaborated upon, aloing with ample illustrations and examples. This section focuses on assorted examples of nonlinear analysis of real-time data from nature, using various tools including as the solitary wavelet, time series, Fourier spectrum, Bispectrum, Spatiotemporal patterns, phase portraits, polar plots, Kolmogorov Entropy, Fractal Dimension, Lyapunov exponents, distance and recurrence plots. These results stand a testimony to the ubiquity of solitons and chaos, and by extension, nonlinearity in the universe.

1. The open circuit photovoltaic output of a solar cell is seen to exhibit a highly fluctuating offset above a fixed DC value. Nonlinear analysis shows this fluctuation to be a highly unstable form of chaos, which is illumination dependent. Moreover, it is seen that this chaotic component shows marked responses in spectral profile to the occurrence of solar flares. Application of the NIST test suite confirmed the random nature of the chaotic signal.

Parameter	Bright	Secondary	Dark
Open Circuit Voltage (DC)	5.25V	1.8V	0.7V
Short Circuit Current	24mA	320uA	10uA
K2 (Nats/Symbol)	17.3975	11.632	7.323
D2 (Dimension)	0.9863	0.9569	0.9684
LLE	7.2438	10.0791	7.2529

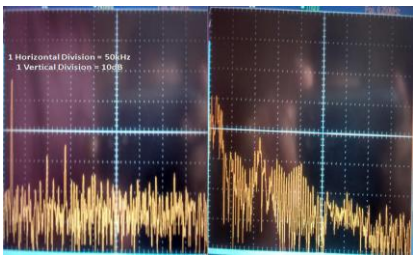

Figure 42 Setup, characterization and spectral profile during low (left) and high (right) solar flare activity

2. The analysis of more than 300 ElectroEncephaloGram (EEG) signal samples taken during normal activity, seizure activity and epileptogenic region EEG during normal activity reveals that seizure EEG spectra, to a greater extent, and non-seizure epileptogenic EEG spectra, to a lesser extent, display prominent high frequency peaks, suggestive of resonant behavior [60]. Nonlinear analysis using phase portraits too confirm the resonance oriented periodic orbits seen in Seizure EEG. Quantitative analysis performed using Largest Lyapunov Exponents (LLE) and Fractal Dimension (D) reveal that both D and LLE values for seizure EEG are much lower than the healthy counterparts, with non-seizure epileptogenic EEG D and LLE values seen somewhere in between. The essence of these results is the observation of a distinct, uniquely identifiable low-dimensional chaotic behavior in EEG taken from epileptogenic region during non-seizure activities. This information can be used both as a preventive epilepsy diagnostic technique, as well as a post-surgical recovery assessment tool.

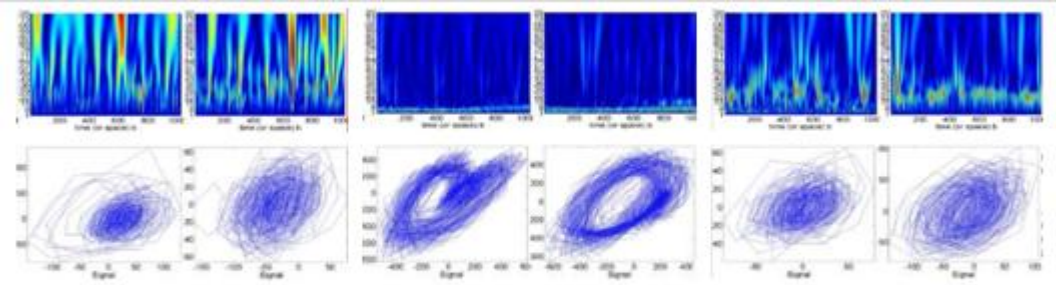

Solitary Wavelet (above) and Phase Portrait (below) analysis for healthy EEG (left, LLE:4.34), epileptic seizure-activity EEG (middle, LLE:0.34) and epileptogenic region normal activity EEG (right, LLE:1.74)

Figure 43 Wavelet and phase portrait analysis of EEG signals

3. It is well known that the variations in frequencies (Swaras) and timbre (tone) form melody (Raga), the key aspect leading to all kinds of music experience. The pinnacle of exploring the frequencies within an octave is the Melakartha system of Carnatic Music. A time domain waveform of the Swara is used to form an iterative map explaining the evolution and behavior of the Raga, and thus music experience. The presence of sensitivity, or chaotic behavior is seen and studied using phase portraits, maximal Lyapunov Exponents and Distance Plots.

$$R_n = R_{n-1} - \sum_{j=1}^{12} \frac{M(j) f_s(j)}{2.4790} \sum_{i=1}^{4} 2\pi\, i\, A_i \sin(2\pi i\, f_s(j) n)$$

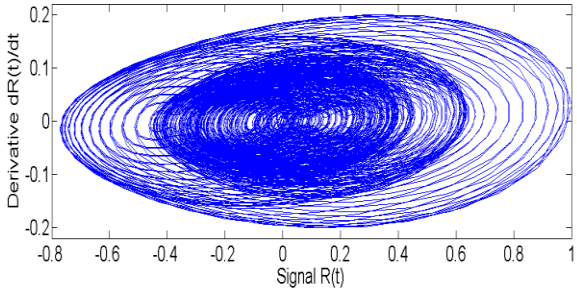

Figure 44 Iterative Map and Phase Portrait of the 'Raga' experience relation

4. The Game of Life is arguably the most popular and productive cellular automaton ever discovered, with applications in evolutionary dynamics and Turing Machine Designs [61]. A Sense Enhanced Game of Life (SEGoL) is introduced, which is essentially the original GoL

including sense enhanced perceptibility. To achieve this, two grids, namely the Life Grid L and the Sense Grid S are defined, with L taking one of two values (alive or dead) and S taking one of three values (touch, sight and sound), with the value in a particular S grid affecting the neighborhood perceptibility in the corresponding S grid. Based on the design, the evolutionary patterns are studied for various rules, coupled with the entropy values and survival rates. Among various cases explored, certain interesting cases leading to self-organization in the sense grids, with or without accompaniment of clustering of certain senses are observed. Figure shows the life and sense grids, illustrating the clustering for random initiation with a rule set R={a,b,c,d,F0,F1,F2}={[3],[2,3],[0,4],[4,8],[2,3],[0,5],[5,8]} where a, b, c, d correspond to sight upgradation, sound upgradation, sight retention and sound retention and F0, F1 and F2 corresponding to life retention in touch, sight and sound cases respectively.

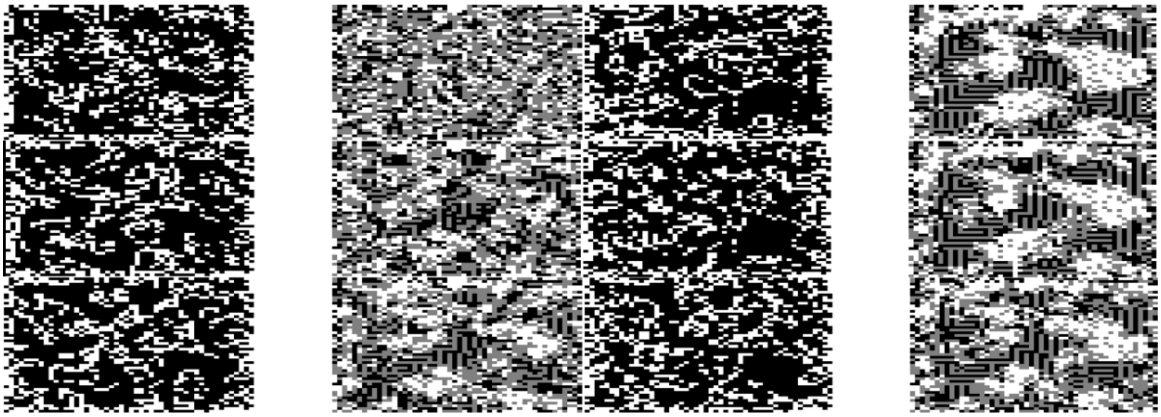

Figure 45 Life (left) and Sense (right) grids for SEGoL with rule R2

5. Nonlinear analysis of radio astronomical data reveal that some of the signals such as the Saturn rotation, Jovian electron cyclotron and Earthquake recordings show highly chaotic nature, as seen by the positive LLE value [62]. Furthermore, polar plot of the B1933 pulsar data shows precise angles at which beaming occurs, apart from distinctly separating the pulses from the noise floor.

Description	K2 (nats/symbol)	D2	LLE
Jupiter hiss recording at 25.55 and 25.67 MHz by Altaïr	0.968	0.79	0.12
Lightning in Jupiter's atmosphere recorded by plasma wave instrument onboard Voyager's spaceprobes	0.886	0.66	-0.61
Jovian electron cyclotron emission	1.008	0.99	7.66
Mixed of Jupiter L-burst and Io B-storm recorded in stereo on March 7, 2001 at 0247 UTC by Thomas Ashcraft	0.928	0.90	-0.21
The sound of Saturn rotation, recorded over a five day interval, from 2-7 June 2004 during Cassini-Huygens approach to Saturn. These low frequencies radio emissions called Saturn Kilometric Radiation (SKR) are generated by charged particles whose motions are controlled by the planetary magnetic field.	0.896	0.85	23.49
Cosmic background noise recorded in the hydrogen line on 1420.40575 MHz. Recorded in the framework of SETI project Argus.	0.843	0.79	-0.47
Earthquake Recording	1.026	0.66	6.94
A type III solar burst on November 4, 2003 by Cassini spaceprobe, produced by very energetic (1 to 100 keV) electrons emitted by a solar flare.	0.883	0.95	0.23
"Saucers" recorded by Dynamics Explorer spacecraft.	1.173	0.66	0.29
Dawn chorus with evident magnetic field micro-pulsations (undulations in the chorus trains).	1.03	0.66	2.25

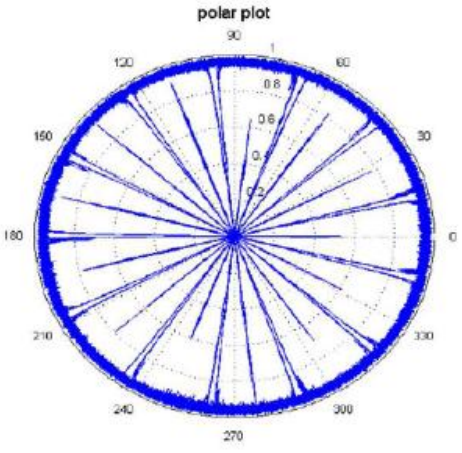

Figure 46 Nonlinear Analysis in Radio Astronomy data

6. Nonlinear analysis also finds fruitful applications in biochemistry and material science. Specifically, by analyzing the Voltage-Resistance and Voltage-Capacitance plots of a cyclic voltammetry result of chrysin and chrysin-copper and iron complex reaction with lipid bilayer membranes, one observes hysteresis behavior characterized by negative resistance peaks for certain concentrations [63]. The LLE values are illustrated below. Similarly, the transient response of Gallium Oxide based thin film ammonia gas sensor reveals concentration dependent resistance variation, with finite response and recovery times. The Lyapunov Exponents computed indicate an optimum ammonia concentration of 5ppm maximizing the sensitivity with optimal response and recovery times [64]. This plot is shown below. The principles of scattering and nonlinear analysis are also put to good use in a novel microwave based material characterization technique. By connecting a klystron based microwave source to a transmitter antenna, a turn table rotates the sample to be characterized, placed in the radiation field of the antenna, by 360 degrees. A receiver antenna then collects the scattered radiation, and the distribution of intensity for various angles is recorded using power meter. Nonlinear analysis techniques such as spectrum, phase portrait, polar plot and Lyapunov exponents are then used to characterize the crystalline/amorphous nature of the sample. The techniques are validated for nanostructured samples of Titanium Oxide as well as Zinc Oxide based thin films. It is hoped that these preliminary results will lay the foundation steps towards microwave based material characterization, with the significant advantage of lesser health hazard compared with X-Ray based techniques. The schematic and nonlinear analysis results for TiO_2-on-Ti thin film, metal side facing transmitter are shown below.

Concentration (μM)	Chrysin	Chrysin-Copper	Chrysin-Iron
0	4.15	4.24	5.82
20	4.12	4.32	5.63
40	4.02	4.37	5.72
60	4.12	4.28	5.64
80	4.07	4.31	5.85
100	4.09	4.25	5.92

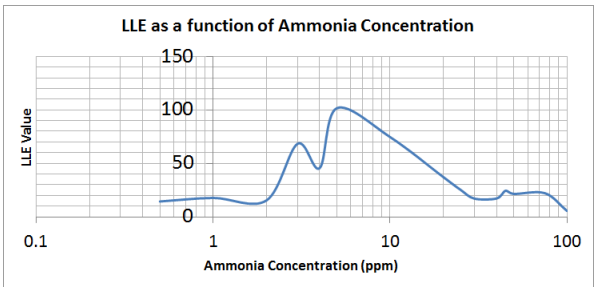

Figure 47a LLE values for Chrysin-lipid bilayer interaction and ammonia gas sensing

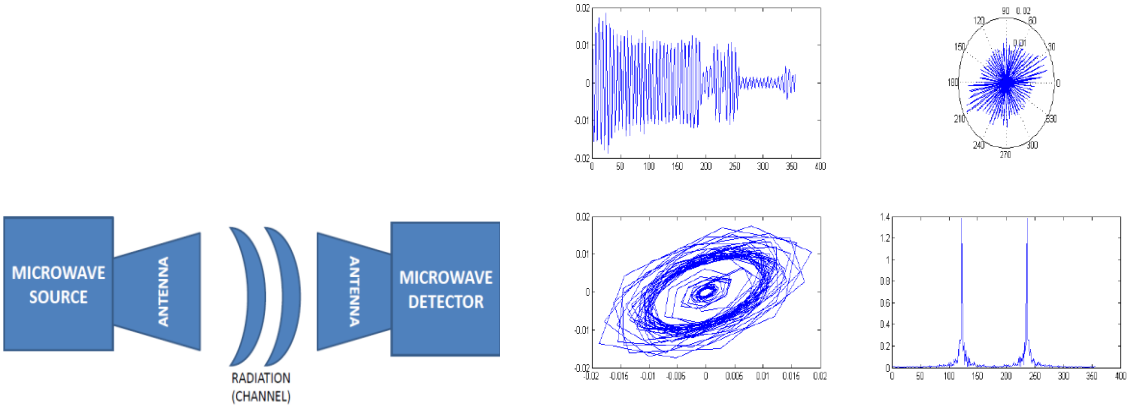

Figure 48b Material Characterization using microwaves

7. The Annual Growth Rate of Gross Domestic Product of an economy is often seen as a key indicator to the economy's growth and prosperity. Nonlinear analysis is performed on the GDP growth data of nations and supranational entities using two key tools, namely Averaged Lyapunov Exponent (ALE) and Distance Plot. The analyses ascertain the presence of chaos in the GDP growth rate data for both nations and supranational entities [65]. Following this, some key inferences from the nonlinear analysis are presented, such as the high value of ALE obtained for fragile and conflict ridden economies, indicating the relationship between ALE and instability, the ALE analysis of BRICS nations as well as low ALE values of supranational entities such as OECD and EU. It is opined that the obtained results pave the way for unlocking a wealth of information regarding GDP growth rates ushering in a new era of 'Smart Economics'. As an illustration, the Distance plot analysis of India's GDP is plotted.

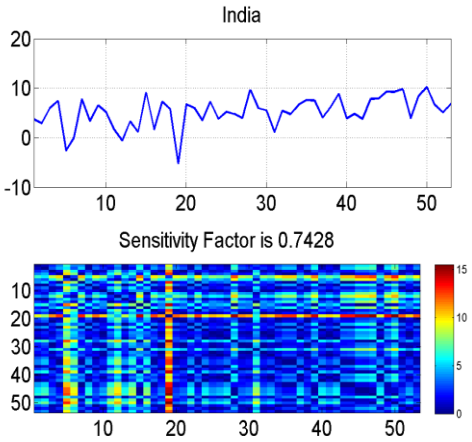

Supra National Entity	ALE	Supra National Entity	ALE
Arab World	0.92375	Low and Middle Income	0.2913
Caribbean Islands	1.06115	Low Income	0.38925
Central Europe and Baltic	1.115	Lower Middle Income	0.338
East Asia and Pacific - All	0.0944	Middle East and North Africa - All	0.7135
East Asia and Pacific - Developing	0.4293	Middle East and North Africa - Developing	0.96715
Euro Nations	0.2184	Middle Income	0.2788
Europe and Central Asia - All	0.233	North America	0.3557
Europe and Central Asia - Developing	1.35985	OECD Countries	-0.0402
European Union	0.1669	Pacific Islands	0.82725
Fragile and Conflict Affected Nations	1.645	North Asia (Russia)	1.47965
Heavily Indebted Poor Countries	0.2783	Small States	0.6517
High Income	1.32705	South Asia	0.5541
OECD High Income	-0.0152	Sub Saharan Countries – All	0.4202
Latin America and Caribbean - All	0.5982	Sub Saharan Countries - Developing	0.4563
Latin America and Caribbean - Developing	0.65	Upper Middle Income	0.3295
Least Developed	0.67135	World	0.0493

Figure 49 Nonlinear Analysis of GDP Growth Rate of India and supranational entities

8. Nonlinear Analysis also finds application in assessing public sentiment about a corporation using its share revenue data, and connecting it with important HR and strategic decisions made within the organization such as announcements of hikes, dividends and layoffs [66]. As an example, the solitary wavelet analysis and quantitative analyses of the share revenue of a Fortune 500 organization during a major layoff operation is shown. The extremely high sensitivity shown by the LLE value of several hundreds, heightened even more during the layoff, as well as the "black mark" seen in a localized scale in the wavelet analysis illustrate the extent of public sentiment influence due to the layoff decision.

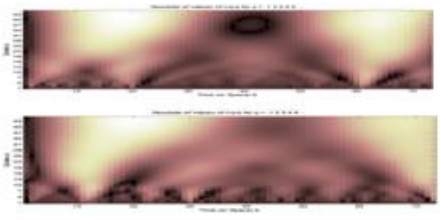

		DURING	AFTER
SHARE PRICE	LLE	31.67	16.77
	D2	0.68	0.68
	K2	4.28	4.29
SHARE REVENUE	LLE	500	707
	D2	0.68	0.68
	K2	4.23	4.21

Multiscale and Quantitative nonlinear analysis of share price and revenue time series during layoff

Figure 50 Nonlinear Analysis of Share Revenue Data during layoff operations

9. Nonlinear Analysis also finds applications in Satellite Imagery data. As an example, the entropies and fractal dimensions of satellite imagery data of various Indian states are illustrated in Fig. 49, and from the results it is seen that sharp and rich variations in terrain from green to arid or snow-clad mountainous regions contribute to high entropy, while rich variations in borders and varying scales of vegetation patches correspond to high fractal dimensions. In a similar fashion, an unprecedented exploration of nonlinear analysis in two geography-oriented disciplines – cartography and vexillology is carried out [67]. Specifically, the tools of fractal dimension and entropy are used to characterize the outline of around 200 countries, following which entropy for the red, green and blue color distributions of the corresponding flags are computed. Key inferences are listed, one of which is the remarkable correlation observed in all cases between the three entropies, as illustrated.

State	E	D	State	E	D
Andhra Pradesh	6.6818	1.6962	Manipur	6.4657	1.6962
Arunachal Pradesh	7.2466	1	Meghalaya	6.4214	0.7925
Assam	6.7967	1.661	Mizoram	5.8658	0.7925
Bihar	6.6301	1.4534	Nagaland	6.7092	1.6962
Chattisgarh	6.5141	1.661	Odisha	6.6284	1.585
Goa	5.9606	1.7925	Punjab	6.5486	1.6962
Gujarat	6.8047	1.4534	Rajasthan	7.066	1.585
Haryana	6.667	1	Sikkim	7.7576	1.6962
Himachal Pradesh	7.6382	1.6962	Tamilnadu	6.9439	1.7925
Jammu & Kashmir	7.5337	1.5646	Telangana	6.7456	1.585
Jharkhand	6.4915	1.5646	Tripura	6.3188	1
Karnataka	6.6426	1	Uttar Pradesh	6.9518	1.4534
Kerala	6.5025	1.661	Uttarakhand	7.3694	1.4534
Madhya Pradesh	6.5671	1.4534	West Bengal	6.8436	1.661
Maharashtra	6.4231	1.4534			

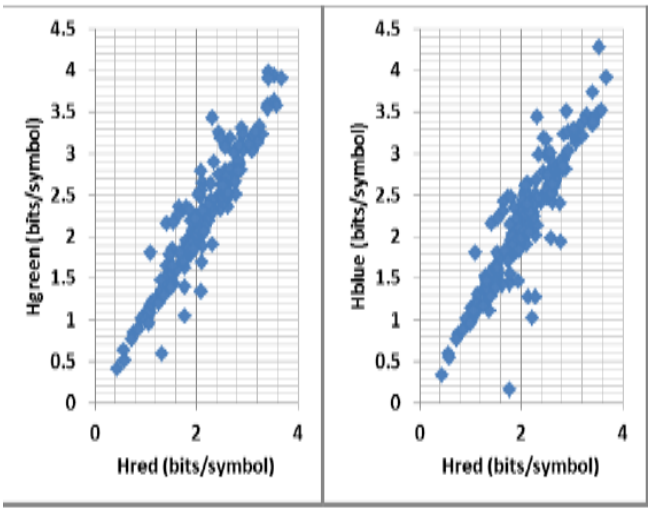

Figure 51 Nonlinear Analysis in satellite imagery, cartography and vexillology

10. A key case of nonlinearity lies in intermodulation distortion, essentially intermixing of two input signals to produce sum and difference frequencies along with various harmonics, caused in passive planar microwave interconnects in integrated circuit back end of lines due to the undesirable phenomenon of self-heating. The concept is outlined briefly as follows. The collision of charge carriers in a resistive element causes change in temperature and this change is periodic, with a baseband range. When a 2 tone input signal is given as input, the power spectrum consists of the sum (f1 + f2) and the difference (f1 − f2), also called envelope or beat frequency. If the beat frequency happens to fall in the thermal baseband range, the thermal effects become prominent, periodically varying the resistance. In effect, this creates a parasitic passive mixer effect producing intermodulation distortion through upconversion of the envelope frequencies at baseband to RF frequencies. Combining the temperature dependent resistivity and heat conduction equations, one gets $\nabla.\left(\frac{\Delta(I^2RT)}{\Delta T}\right) - C_v\frac{\partial T}{\partial t} = J^2[\rho_0(1+\alpha T+\beta T^2+\cdots)]$. This yields an equivalent representation of self-heating by a parallel RC circuit given by $R=1/kC_v$; $C=C_vR$ with k signifying diffusibility. By representing microstrip interconnect geometries as equivalent RLC transmission line models and coupling this model to the self heating equivalent circuit, one obtains a plot of IMD3 versus separation in input frequencies, when driven by a two tone input

signal. This is illustrated for various conductor and substrate material configurations. Of particular mention are self-heating and device nonlinearities leading to power quality problems in voltage distribution load systems. Filtering of such harmonics can be done effectively using lumped low pass filters with planar configurations, where strip line inductors are used in conjunction with a fractal interdigitated capacitor comprising of fused silica strip over ceramic substrate ($La_{0.5}Na_{0.5}Cu_3Ti_4O_{12}$) possessing extremely high dielectric constant (ε_r=1,00,000). A tabulation of the Total Harmonic Distortion achieved with and without using the proposed filter in a single phase full wave diode bridge rectifier is illustrated.

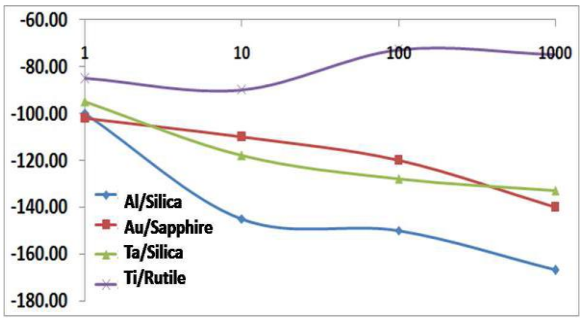

Load parameters	Without filter (%)	With Filter (%)
R_{load}=10 ohm and C_{load} = 220 μF	52.85	1.97
R_{load}=10 ohm and C_{load} = 470 μF	50.85	2.07
R_{load}=10 ohm and C_{load} = 740 μF	48.59	2.38
R_{load}=20 ohm and C_{load} = 220 μF	54.63	2.84
R_{load}=20 ohm and C_{load} = 470 μF	52.82	2.94
R_{load}=20 ohm and C_{load} = 740 μF	52.70	3.09
R_{load} =32 ohm and C_{load} = 220 μF	55.59	3.21
R_{load} =32 ohm and C_{load} = 470 μF	54.56	3.33
R_{load} =32 ohm and C_{load} = 740 μF	68.30	3.44

Figure 52 Self Heating Induced IMD3 and planar harmonic elimination filter results

5. Conclusion

In the present work, the underlying philosophies of two pinnacles of nonlinearity, namely solitons and chaos are discussed. In short, the soliton is viewed as the very representative of the life process comprising of birth, growth, zenith, decay and death. Various applications of the soliton in communications and computing are discussed. The smoothness and compactness of the soliton give rise to its involvement in various phenomena in nature, along with the genesis of the 'solitary wavelet'. With the characteristic signatures of determinism and sensitive dependence on initial conditions, chaos theory forms the hallmark of nonlinear science. The present work stresses on and elaborates various techniques on achieving an easy-to-tune signal based chaos, with the help of standard circle maps, mathematical functions and digital circuits. Following this various applications of chaos theory are discussed, culminating in a chaotic interpretation of quantum mechanics and Theory of Everything. Finally, nonlinear analysis and its significance in various real time data is outlined.

As a concluding exercise, I turn towards spirituality, where an assortment of Naamas from the Lalitha Sahasranama pertaining to nonlinearity and cosmology are presented, with interpretations guided by of decipherments of metaphors, allusions, symbolism, semiotics and etymo-linguistic studies [68].

The first few Naamas of the Lalitha Sahasranama are presented as a narration of how the Divine Mother Lalitha slays the evil Bhandasura, who is a metaphor for ignorance. It is seen that the only way out of ignorance is willingness to know; in other words, the awareness and consciousness required to know. This fundamental consciousness is seen as the Divine Mother Lalitha. Thus Bhandasura represents the empty void of the universe, in complete darkness and inconceivable inertia. The Divine Mother is the pure consciousness, the powerful information that quells the darkness of ignorance. It is this information that

makes up the universe. The first few Namas denote the Five great actions performed by the Mother, simultaneously alluding to key paradigms in science and management.

A. SHRI MATHA: The Mother. The source of all creation. The Ma in Matha signifies enlightenment whereas the A symbolizes bliss. Enlightenment denotes that the first wave of creation was one of information. The action alluded to is Srishti – Creation.
B. SHRI MAHARAJNI: The Supreme Empress. The only One that has ever been, and the only One that ever will be. This can be taken by extension to categorically dispel off multiverse theories of everything, signifying that our Universe may be the only One. The action here is Sthithi – Preservation.
C. SHRIMATH SIMHAASANESHWARI: The One with a Lion Seat. Lion alludes to might, valour and destruction. The action here is Samhaara – Destruction.
D. CHIDAGNI KUNDA SAMBHOOTHA: The One emergent from the Fire-pit of Consiousness. This clearly demonstrates the equivalence of information (consciousness Chid) and energy (fire Agni). Coupled with Einstein's famous Mass-Energy equivalence, information can be shown to be the basic constituent of all matter and energy in the Universe. The action here is Tirodhaana – Compactification.
E. DEVAKAARYA SAMUDBHAVA: The One arising of Divine Act. Mythologically it alludes to the various Gods (Devas) invoking Lalitha. This Nama summarises the key intent of the Universe in a single word – Divine. Divine intent is defined to be the intent that maximizes the welfare of the whole universe. The action here is Anugraha – Grace.
F. UDYADBHAANU SAHASRAABHA – One with the splendor of a 1000 rising suns. This Nama refers to the radiance of the Divine Mother. Also, it alludes to the fact that during Creation (Udyad), when there was only information, the energy equivalence of that consciousness was extremely high. This is noteworthy because Particle Physics researches such as the CERN in Geneva conduct experiments in the range of Giga and Tera Electron Volts (GeV-TeV) to detect subatomic particles and confirming theories corresponding to early stages of our universe [69-71].
G. CHATURBAAHU SAMANVITHA: The Four Armed One. The four arms here clearly refer to the four principal dimensions of the world we live in – three space dimensions (length, breadth and height) and one time dimension. The theory of General Relativity has explored in detail this 4D spacetime construct and has clearly shown that it is these dimensions and the way they interact with matter that are responsible for mass and gravity.

The next few Namas enumerate the Ayudhaas or Tools in the four hands of the Divine Mother.

H. RAAGASVAROOPA PAASHAADYA KRODHAANKAARAAKUSHOJJVALA: The One who has the Noose of Desire and the Goad of Hatred. The first two 'weapons' listed are love and hatred. It is well known from psychology that love and hatred arise due to discrimination – we valuate something either exceptionally higher or lower than others, causing us to love or hate it respectively. Thus, the key element here is discrimination. Mathematically, this discrimination is termed Nonlinearity, and it is easy to see why it is essential. Without discrimination, one would neither have pleasure and pain. Insects and reptiles would be gnawing away at flesh and bones and one would neither feel pain nor know a thing. Without the sharp nonlinearity at 100 degrees

Celsius, water would boil just at any temperature, which means that most of our body constituents would be an incoherent mess, without form or structure.

I. MANOROOPEKSHU KODANDA PANCHATANMAATRA SAAYAKA: The One wielding the Bow of the Mind and the Five Arrows of the Senses. If the form of the Mother and hence of the Universe is indeed information, then it is imperative to have a receptor. Of what use is information without something to perceive it? This receptor is the most beautiful organ in nature – the mind. One might ask an intuitive question: The mind is also a thing in this universe, hence made up of information. How then does information detect information? Here the essential ingredient for information A to perceive information B is complexity. The complex one will perceive the simple one, but not vice versa. Thus the principal characteristic of the mind is complexity of information. Mathematically, this complexity of information is called Chaos. Recent studies of EEG brain waves completely testify to the fact that the dynamics of the mind are indeed chaotic [72-74]. The Five Senses allude to the various forms by which information is perceived by the mind. In other words, it tells us the forms of information, which can be alternatively viewed as the dimensions of information. These higher dimensions of information compactify into various properties like color, texture, charge and mass in our 4D spacetime.

J. NIJARUNA PRABHAPOORA MAJJAD BRAHMAANDA MANDALA: The Radiant Resplendent One with the Hue of the Rising Sun. This verse is an allusion to the geometry (Mandala) of the Universe (Brahmanda). The various descriptions of Higher Dimensions in Modern Physics are represented mathematically as groups of operators. There are many such groups such as U(1), SU(2), SO(2), SU(3), D4, G4 and so on. The largest simple exceptional group is the 8 Dimensional E8. The structure of E8 represents an 8D polytope with 248 symmetries. This E8 appears in the Heterotic String Theory as E8xE8, and the E8 Theory of Everything is completely centered on the E8. This E8 is often described as the most beautiful and intricate mathematical structure.

K. CHAMPAKA ASHOKA PUNNAAGA SAUGANDHIKA LASATKACHA: The One whose Hair is adorned by the four fragrant flowers. The four flowers that adorn Her hair are an allusion to the four families of coordinates in the E8 model. They are Spatio-Temporal (wS and wT), Electroweak (U and V), Coupling (W) and Color (X, Y and Z). These four groups form the basis for defining each elementary particle uniquely in the E8 space.

L. KURUVINDA MANISHRENI KANAT KOTIRA MANDITHA: One whose Crown is adorned by the rare Kuruvinda Ruby. In the Kundalini Yoga, Seven Energy centers of the human body are described, each one associated with a particular world view, color and musical note. Of these, Muladhara, the lowest of these is associated with the Red color, and is also the seat of the Kundalini serpent at the fully evolved state. During spiritual progress, this serpent representing Shakti rises, passes through the seven Chakras, reaching its destination at the Crown, the Sahasrara representing Shiva. This concept is alluded to in this Nama where the ruby (denoting the Kundalini serpent from the Muladhara) is present in the Crown Chakra, representing complete spiritual progress and hence Self-Realisation or Moksha.

M. ASHTAMI CHANDRA VIBRAJA DHALIKA STHALA SHOBITHA: The One whose forehead appears like the eighth day moon. This is again an allusion to the 8 dimensions of the E8 group. Also, it refers to the chemical tendency of elements to attain stability in the half full and full valency states.

N. MUKHACHANDRA KALANKABHA MRUGANAABHI VISHESHAKA: One with the resplendent Kasturi mark. The Kasturi mark is an allusion to the third eye of the Divine Mother. It is mentioned that the Mother's right and left eyes represent the sun and the moon, whereas Her Third Eye represents Fire. Thus, the Kasturi on the third eye denotes symmetry of the first two, and also denotes the equivalence of Information with Force and Matter.

O. VADANASMARA MAANGALYA GRUHA THORANA CHILLIKA: The One whose eyebrows resemble the festoons of Cupid. This Nama alludes to the nature of information-force-matter described in the previous Nama. Specifically, it says that the eyebrows, which seen from afar look like a continuous line, actually resemble a garland (Thorana). This implies that at the smallest scale of space and time, various parameters of the universe such as energy is discrete. This is verily the postulate of Quantum Mechanics and Quantum Field Theory which has been successfully tested rigorously in the past few decades.

P. VAKTRA LAKSHMI PARIVAAHA CHALAN MEENABHA LOCHANA: The One whose Eyes resemble Fish moving Swiftly in a pond. It is well known that a person's emotions can best be ascertained from their eyes. Similarly, the Mother's Eyes, filled with the emotion of Compassion move swiftly so that She casts Her Grace (Kataaksha) on the entire universe. More specifically, this Nama alludes to the Activity modes of the information that make up matter (moon) and energy (sun). This information varies with time, and if the E8 theory is assumed, the information consists of 3 Quantum Bits or Qubits. The activity modes of the 3 qubits are defined as the three Gunas of Sattva, Rajas and Tamas.

Q. NAVACHAMPAKA PUSHPAABHA NAASADANDA VIRAAJITHA: The One whose nose resembles a new blossom of Champaka. The nose is an organ of smell, and the Champaka is the source of a fragrance. By equating the both, this Nama alludes to the fact that the Divine Mother represents ultimate Spiritual transcendence where the worshipper, the worship and the Deity all merge into one single entity. This is verily the principle of Advaita.

R. TAARAAKAANTHI TIRASKARI NAASAABHARANA BHAASURAA: The One wearing a nosestud that outshines the stars. This verse is an allusion to cosmology. The nasal bridge represents a waisted hyperbolic geometry – the deSitter geometry of spacetime with positive curvature. This geometry represents the inflation that occurred in the early universe. Also, the nosestud near the bottom of her nose (end of this inflated stage) represents the various stars, planets and celestial bodies found at the end of inflation. At this stage, the universe consists of three kinds of entities – Ordinary Matter (Non Inflating), Cold Dark Matter (Non Inflating) and Dark Energy (Inflating). While the shape of the nasal bridge alludes to dark energy, Her nostrils and the darkness within alludes to dark matter and the nose stud alludes to ordinary matter, which by size and volume is much smaller than Her nostril (dark matter) [75-79].

The Naama interpretations listed above stand further testimony to the ubiquity and fundamental nature of nonlinearity in the universe. The science world's slumber of linearity was indeed a tad too long [80]. Here is to hoping that nonlinearity doesn't take too long to dawn.

References

[1] Scott, Alwyn C. The nonlinear universe: chaos, emergence, life. Springer Science & Business Media, 2007.

[2] Perovic, Slobodan K. "Emergence, nonlinearity, and living systems: A metaphysical lecture from biology?." (2005).

[3] Tiemeijer, L. F. "Effects of nonlinear gain on four-wave mixing and asymmetric gain saturation in a semiconductor laser amplifier." Applied physics letters 59, no. 5 (1991): 499-501.

[4] Overman, E. Sam. "The new sciences of administration: Chaos and quantum theory." Public Administration Review (1996): 487-491.
[5] Tabor, Michael. Chaos and integrability in nonlinear dynamics: an introduction. Wiley Interscience, 1989.
[6] Holmes, Philip. "Poincaré, celestial mechanics, dynamical-systems theory and "chaos"." Physics Reports 193, no. 3 (1990): 137-163.
[7] Lorenz, Edward N. The essence of chaos. University of Washington Press, 1995.
[8] Strogatz, Steven H. Nonlinear dynamics and chaos: with applications to physics, biology, chemistry, and engineering. Westview press, 2014.
[9] Sawada, Katuro, and Takeyasu Kotera. "A method for finding N-soliton solutions of the KdV equation and KdV-like equation." Progress of Theoretical Physics 51, no. 5 (1974): 1355-1367.
[10] Scott, Alwyn. Nonlinear science. Oxford Univ. Press, 2003.
[11] Hirota, Ryogo. "Exact solution of the sine-Gordon equation for multiple collisions of solitons." Journal of the Physical Society of Japan 33, no. 5 (1972): 1459-1463.
[12] Remoissenet, Michel. Waves called solitons: concepts and experiments. Springer Science & Business Media, 2013.
[13] Akhmediev, N., J. M. Soto-Crespo, and A. Ankiewicz. "Extreme waves that appear from nowhere: on the nature of rogue waves." Physics Letters A 373, no. 25 (2009): 2137-2145.
[14] Chui, Charles K. "Wavelets: a tutorial in theory and applications." Wavelet Analysis and its Applications, San Diego, CA: Academic Press,| c1992, edited by Chui, Charles K. 1 (1992).
[15] Meyer, Yves. "Wavelets-algorithms and applications." Wavelets-Algorithms and applications Society for Industrial and Applied Mathematics Translation., 142 p. 1 (1993).
[16] Sze, Simon Min. Semiconductor devices: physics and technology. John Wiley & Sons, 2008.
[17] Ricketts, David S., Xiaofeng Li, Nan Sun, Kyoungho Woo, and Donhee Ham. "On the self-generation of electrical soliton pulses." Solid-State Circuits, IEEE Journal of 42, no. 8 (2007): 1657-1668.
[18] Willebrand, Heinz, and Baksheesh S. Ghuman. Free space optics: enabling optical connectivity in today's networks. SAMS publishing, 2002.
[19] Al-Raweshidy, Hamed, and Shozo Komaki. Radio over fiber technologies for mobile communications networks. Artech House, 2002.
[20] Kivshar, Yuri S., and Govind Agrawal. Optical solitons: from fibers to photonic crystals. Academic press, 2003.
[21] Mihalache, D. "Linear and nonlinear light bullets: Recent theoretical and experimental studies." Rom. J. Phys 57 (2012): 352-371.
[22] Assanto, Gaetano, Marco Peccianti, and Claudio Conti. "Nematicons: optical spatial solitons in nematic liquid crystals." Optics and photonics news 14, no. 2 (2003): 44-48.
[23] Grelu, Philippe, and Nail Akhmediev. "Dissipative solitons for mode-locked lasers." Nature Photonics 6, no. 2 (2012): 84-92.
[24] Rauch, Jeffrey, and Joel Smoller. "Qualitative theory of the FitzHugh-Nagumo equations." Advances in mathematics 27, no. 1 (1978): 12-44.
[25] Kiehn, R. M. "Falaco Solitons." Cosmic strings in a swimming pool (1987).
[26] Christiansen, Peter L., and Alwyn C. Scott, eds. Davydov's soliton revisited: self-trapping of vibrational energy in protein. Vol. 243. Springer Science & Business Media, 2013.
[27] Gariaev, Peter, Boris I. Birshtein, Alexander M. Iarochenko, Peter J. Marcer, George G. Tertishny, Katherine A. Leonova, and Uwe Kaempf. "The DNA-wave biocomputer." In The fourth international conference on computing anticipatory systems (CASYS), Liege. 2000.
[28] Burger, Stefan, K. Bongs, S. Dettmer, W. Ertmer, K. Sengstock, A. Sanpera, G. V. Shlyapnikov, and M. Lewenstein. "Dark solitons in Bose-Einstein condensates." Physical Review Letters 83, no. 25 (1999): 5198.
[29] Constantin, Adrian, and David Henry. "Solitons and tsunamis." Zeitschrift für Naturforschung A 64, no. 1-2 (2009): 65-68.
[30] Nucamendi, Ulises, and Marcelo Salgado. "Scalar hairy black holes and solitons in asymptotically flat spacetimes." Physical Review D 68, no. 4 (2003): 044026.
[31] Rosenstein, Michael T., James J. Collins, and Carlo J. De Luca. "A practical method for calculating largest Lyapunov exponents from small data sets." Physica D: Nonlinear Phenomena 65, no. 1 (1993): 117-134.
[32] Wolf, Alan, Jack B. Swift, Harry L. Swinney, and John A. Vastano. "Determining Lyapunov exponents from a time series." Physica D: Nonlinear Phenomena 16, no. 3 (1985): 285-317.
[33] Phatak, S. C., and S. Suresh Rao. "Logistic map: A possible random-number generator." Physical review E 51, no. 4 (1995): 3670.
[34] Devaney, Robert L. An introduction to chaotic dynamical systems. Vol. 13046. Reading: Addison-Wesley, 1989.
[35] Bilotta, Eleonora, and Pietro Pantano. A gallery of Chua attractors. Singapore: World Scientific, 2008.
[36] Gilmore, Robert, and Marc Lefranc. The topology of chaos: Alice in stretch and squeezeland. John Wiley & Sons, 2012.
[37] Cox, Ingemar, Matthew Miller, Jeffrey Bloom, Jessica Fridrich, and Ton Kalker. Digital watermarking and steganography. Morgan Kaufmann, 2007.
[38] Kaur, Amandeep, and Vinay Chopra. "A Comparative Study and Analysis of Image Restoration Techniques Using Different Images Formats." International Journal for Science and Emerging Technologies with Latest Trends 2, no. 1 (2012): 7-14.
[39] Liao, Samuel Y. "Microwave devices and circuits." Englewood Cliffs: Prentice-Hall, 1985, 2nd ed. 1 (1985).
[40] Barnsley, Michael F. Fractals everywhere. Academic press, 2014.
[41] Mandelbrot, Benoit. Fractals and chaos: the Mandelbrot set and beyond. Vol. 3. Springer Science & Business Media, 2013.
[42] Berndt, Bruce C. "Ramanujan's theory of theta-functions." (1993).
[43] Zagier, Don. "Ramanujan's mock theta functions and their applications." Astérisque 326 (2009): 143-164.
[44] Ono, Ken, and Kannan Soundararajan. "Ramanujan's ternary quadratic form." Inventiones mathematicae 130, no. 3 (1997): 415-454.
[45] Temme, Nico M. "On the numerical evaluation of the modified Bessel function of the third kind." Journal of Computational Physics 19, no. 3 (1975): 324-337.
[46] Greene, Richard F., and Herbert B. Callen. "On the formalism of thermodynamic fluctuation theory." Physical Review 83, no. 6 (1951): 1231.

[47] Yates, Robert Carl. A Handbook on curves and their properties. JW Edwards, 1947.
[48] Kaneko, Kunihiko. "Pattern dynamics in spatiotemporal chaos: Pattern selection, diffusion of defect and pattern competition intermettency." Physica D: Nonlinear Phenomena 34, no. 1 (1989): 1-41.
[49] James, Ryan G., Korana Burke, and James P. Crutchfield. "Chaos forgets and remembers: Measuring information creation, destruction, and storage." Physics Letters A 378, no. 30 (2014): 2124-2127.
[50] Rukhin, Andrew, Juan Soto, James Nechvatal, Miles Smid, and Elaine Barker. A statistical test suite for random and pseudorandom number generators for cryptographic applications. Booz-Allen and Hamilton Inc Mclean Va, 2001.
[51] Langmead, Ben, Cole Trapnell, Mihai Pop, and Steven L. Salzberg. "Ultrafast and memory-efficient alignment of short DNA sequences to the human genome." Genome biol 10, no. 3 (2009): R25.
[52] McMahon, David. Quantum computing explained. John Wiley & Sons, 2007.
[53] Wolfram, Stephen. A new kind of science. Vol. 5. Champaign: Wolfram media, 2002.
[54] Abbott, Derek, Paul CW Davies, and Arun K. Pati. Quantum aspects of life. Imperial College Press, 2008.
[55] Jammer, Max. "Philosophy of quantum mechanics. The interpretations of quantum mechanics in historical perspective." (1974).
[56] Griffiths, David Jeffery. Introduction to quantum mechanics. Pearson Education India, 2005.
[57] Lloyd, Seth. "A theory of quantum gravity based on quantum computation." arXiv preprint quant-ph/0501135 (2005).
[58] Borsten, L., M. J. Duff, and P. Levay. "The black-hole/qubit correspondence: an up-to-date review." arXiv preprint arXiv:1206.3166 (2012).
[59] Lisi, A. Garrett. "An exceptionally simple theory of everything." arXiv preprint arXiv:0711.0770 (2007).
[60] Babloyantz, Agnessa, and Alain Destexhe. "Low-dimensional chaos in an instance of epilepsy." Proceedings of the National Academy of Sciences 83, no. 10 (1986): 3513-3517.
[61] Conway, John. "The game of life." Scientific American 223, no. 4 (1970): 4.
[62] Wilson, Thomas L., Kristen Rohlfs, and Susanne Hüttemeister. Tools of radio astronomy. Vol. 86. Berlin: Springer, 2009.
[63] Selvaraj, Stalin, Sridharan Krishnaswamy, Venkappayya Devashya, Swaminathan Sethuraman, and Uma Maheswari Krishnan. "Investigations on membrane perturbation by chrysin and its copper complex using self-assembled lipid bilayers." Langmuir 27, no. 21 (2011): 13374-13382.
[64] Pandeeswari, R., and B. G. Jeyaprakash. "High sensing response of β-Ga 2 O 3 thin film towards ammonia vapours: Influencing factors at room temperature." Sensors and Actuators B: Chemical 195 (2014): 206-214.
[65] Kříž, Radko. "Chaotic analysis of the GDP time series." In Nostradamus 2013: Prediction, Modeling and Analysis of Complex Systems, pp. 353-362. Springer International Publishing, 2013.
[66] Wheatley, Margaret J. Leadership and the new science: Discovering order in a chaotic world. ReadHowYouWant. com, 2010.
[67] Whyte, Brendan. "On Cartographic Vexillology." Cartographica: The International Journal for Geographic Information and Geovisualization 42, no. 3 (2007): 251-262.
[68] V Ravi, Lalitha Sahasranamam, Manblunder, 2010
[69] Dittmar, Michael, and Herbi Dreiner. "How to find a Higgs boson with a mass between 155 and 180 GeV at the CERN LHC." Physical Review D 55.1 (1997): 167.
[70] Arnison, G., et al. "Experimental observation of lepton pairs of invariant mass around 95 GeV/c 2 at the CERN SPS collider." Physics Letters B 126.5 (1983): 398-410.
[71] Antoniadis, Ignatios. "A Possible new dimension at a few TeV." Physics Letters B 246.3 (1990): 377-384.
[72] Jansen, B. H. "Is it and so what? A critical review of EEG chaos." Measuring chaos in the human brain (1991): 49-82.
[73] Pijn, Jan Pieter, et al. "Chaos or noise in EEG signals; dependence on state and brain site." Electroencephalography and clinical Neurophysiology 79.5 (1991): 371-381.
[74] Pritchard, Walter S., and Dennis W. Duke. "Measuring chaos in the brain: a tutorial review of nonlinear dynamical EEG analysis." International Journal of Neuroscience 67.1-4 (1992): 31-80.
[75] De Sitter, Willem. "Einstein's theory of gravitation and its astronomical consequences. Third paper." Monthly Notices of the Royal Astronomical Society 78 (1917): 3-28.
[76] Witten, Edward. "Anti de Sitter space and holography." arXiv preprint hep-th/9802150 (1998).
[77] De Sitter, Willem. "On the relativity of inertia. Remarks concerning Einstein's latest hypothesis." Proc. Kkl. Akad. Amsterdam 19 (1917): 1217-1225.
[78] Clowe, Douglas, et al. "A direct empirical proof of the existence of dark matter." The Astrophysical Journal Letters 648.2 (2006): L109.
[79] Copeland, Edmund J., Mohammad Sami, and Shinji Tsujikawa. "Dynamics of dark energy." International Journal of Modern Physics D 15.11 (2006): 1753-1935.
[80] Capra, Fritjof. The Tao of physics: An exploration of the parallels between modern physics and eastern mysticism. Shambhala publications, 2010.